Planet. Space Sci., Vol. 33, No. 6, pp. 685–709, 1985
Printed in Great Britain.

0032–0633/85 $3.00 + 0.00
Pergamon Press Ltd.

THE MOTION OF LITHIUM TEST IONS IN THE QUIET TIME NIGHTSIDE MAGNETOSPHERE: CONSERVATION OF MAGNETIC MOMENT AND LONGITUDINAL INVARIANTS

S. C. CHAPMAN and S. W. H. COWLEY
The Blackett Laboratory, Imperial College of Science and Technology, London SW7 2BZ, U.K.

(*Received in final form* 19 *November* 1984)

Abstract—One of the active experiments to be performed as part of the AMPTE mission involves the release of lithium ions in the geomagnetic tail and their subsequent detection after Earthward convection into the nightside outer ring current region. In a previous paper, the guiding centre trajectories of ions were integrated in a simple two-dimensional model of the quiet time nightside magnetosphere in order to estimate their properties on arrival in the ring current region. In this paper, the validity of the guiding centre approximation is investigated, using full trajectory integrations in a simplified one-dimensional field model. In particular, it is shown to be valid for the lithium ion trajectories in the simple two-dimensional model field over the observed range of quiet time magnetotail field values. Analytical approximations for the properties of ions as they first cross the tail centre plane, and approximate longitudinal invariants of the subsequent Earthward motion are then derived. Finally, by comparison of these with the numerical results it is demonstrated that the speeds and pitch angles of the ions arriving in the ring current region can be predicted analytically to a reasonable approximation, and hence can be simply calculated for any given model of the quiet time geomagnetic tail.

1. INTRODUCTION

One of the principal experiments of the Active Magnetospheric Particle Tracer Explorer (AMPTE) spacecraft mission is the study of lithium releases to be made by the Ion Release Module (IRM) in the quiet time magnetospheric tail, and the subsequent detection of the lithium ions by the Charge Composition Explorer (CCE) after their convection into the ring current region. The release will be made at a downtail distance of $\sim 20\ R_E$ in the plasma sheet region near the centre of the geomagnetic tail, and will result in seeding of the magnetospheric plasma with singly charged lithium ions over a region comparable to the thickness of the quiet time plasma sheet ($\sim 10\ R_E$). Since the resulting lithium ion number densities are $\sim 10^{-5}$ cm^{-3} (Krimigis *et al.*, 1982), giving a mass density that is much smaller than the ambient plasma density, the ions may be regarded as test ions.

In a previous paper (Chapman and Cowley, 1984; to be referred to hereafter as "Paper 1") we presented a brief initial report of a study of lithium test ion behaviour in the quiet time nightside magnetosphere. Ion trajectories were integrated using guiding centre theory in a simple two-dimensional model for the magnetotail, and it was shown that whilst the final ion energies depend principally on the equatorial electric field drift speed in the creation region, the final pitch angles depend sensitively on the position of the creation point. The majority of ions, created where $|B_x| \gg B_z$, become closely field-aligned, whereas those created where $|B_x| \lesssim B_z$ arrive at large pitch angles. It was concluded that under usual conditions, on arrival at the outer ring current region the accelerated ions will form a ~ 10–$20°$ pitch angle collimated beam, with lithium ion energies of ~ 1 keV.

In this paper we shall first briefly review the properties of the model field (Section 2), and ion motion within it (Section 3). In Section 4, we then examine the conditions under which guiding centre theory is valid for these trajectories. Finally, in Section 5, the numerical results are used to investigate the validity of approximate longitudinal invariants of the motion, so that the properties of ions arriving in the ring current region may simply be predicted analytically for any given model for the magnetotail, using the results obtained from the simple model used here.

2. THE FIELD MODEL AND GUIDING CENTRE EQUATIONS OF MOTION

A full description of the field model used here, and of the resulting special properties of the guiding centre motion within it has been given in Paper 1, but the essential features will first be briefly reiterated here for ease of reference.

For simplicity, the magnetic field is chosen to be two-dimensional and planar. The vector potential $A_y(x, z)$ (using usual magnetospheric coordinates) is comprised

of two terms, the first being that of a line dipole located at the origin, and the second representing the contribution of the magnetotail current:

$$A_y(x,z) = -\frac{Kx}{(x^2+z^2)} + CF(x)\,e^{Ax}\cos kz \quad (1)$$

where

$$F(x) = \frac{(x/p)^2}{(1+(x/p)^2)}.$$

The magnetic components are then:

$$B_x(x,z) = -\frac{\partial A_y}{\partial z} = \frac{2Kxz}{(x^2+z^2)^2} + kCF(x)\,e^{Ax}\sin kz \quad (2)$$

and

$$B_z(x,z) = \frac{\partial A_y}{\partial x} = \frac{K(x^2-z^2)}{(x^2+z^2)^2} + C\,e^{Ax} \times\left[AF(x) + \frac{\frac{2x}{p^2}}{(1+(x/p)^2)^2}\right]\cos kz \quad (3)$$

and the parameters in equation (1) were chosen as follows:

$$K = 1500\ \text{nT}\ R_E^2$$

$$A = 0.011\ R_E^{-1}$$

$$C = \frac{264}{\pi} \simeq 84.03\ \text{nT}\ R_E$$

$$k = \frac{\pi}{12} \simeq 0.262\ R_E^{-1}$$

$$p = 6\ R_E.$$

The resulting field lines of the model field, given by the contours A_y = constant, are shown as dashed lines on the ion trajectory plots to follow (Figs. 1 and 2, upper panels). Contours are shown at equal intervals of A_y to give an indication of the field strength.

In the tail proper ($|x| \gg p$) the tail current contribution to the above field varies sinusoidally in the z direction on a scale length $z_m = \pi/2k$ (z_m is the plasma sheet half thickness, taken to be 6 R_E), and exponentially in the x direction on a scale length A^{-1}.

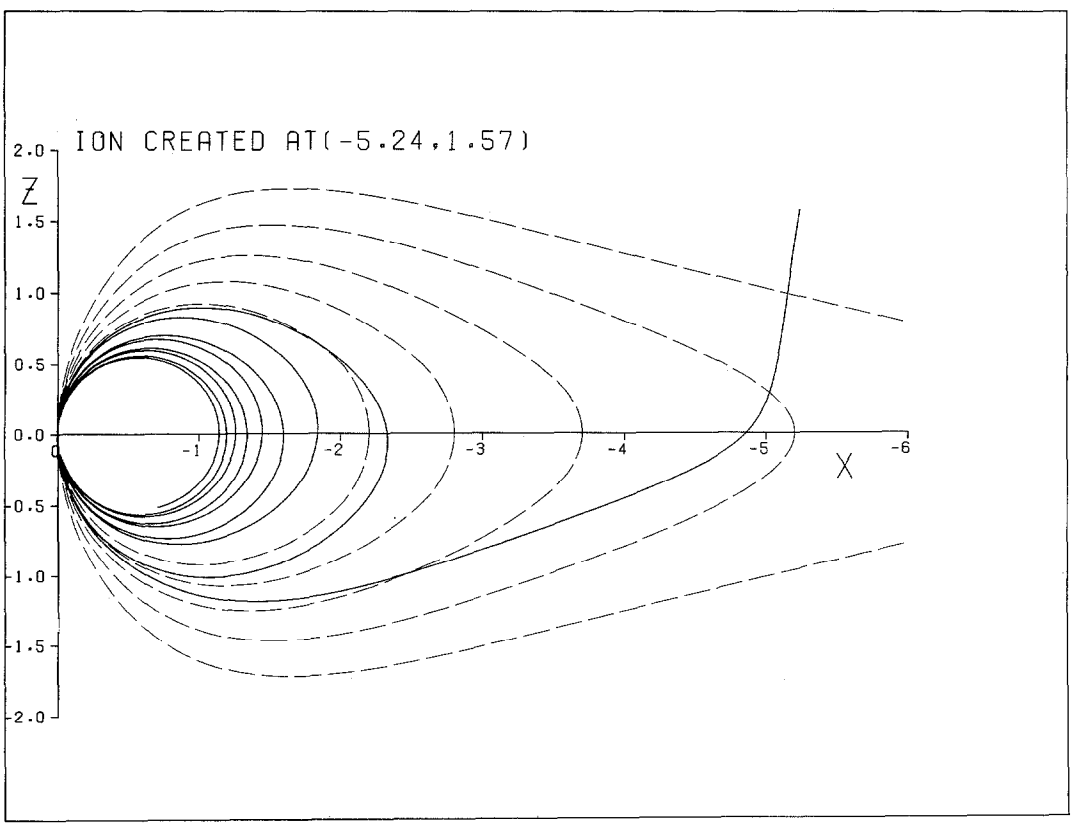

FIG. 1.

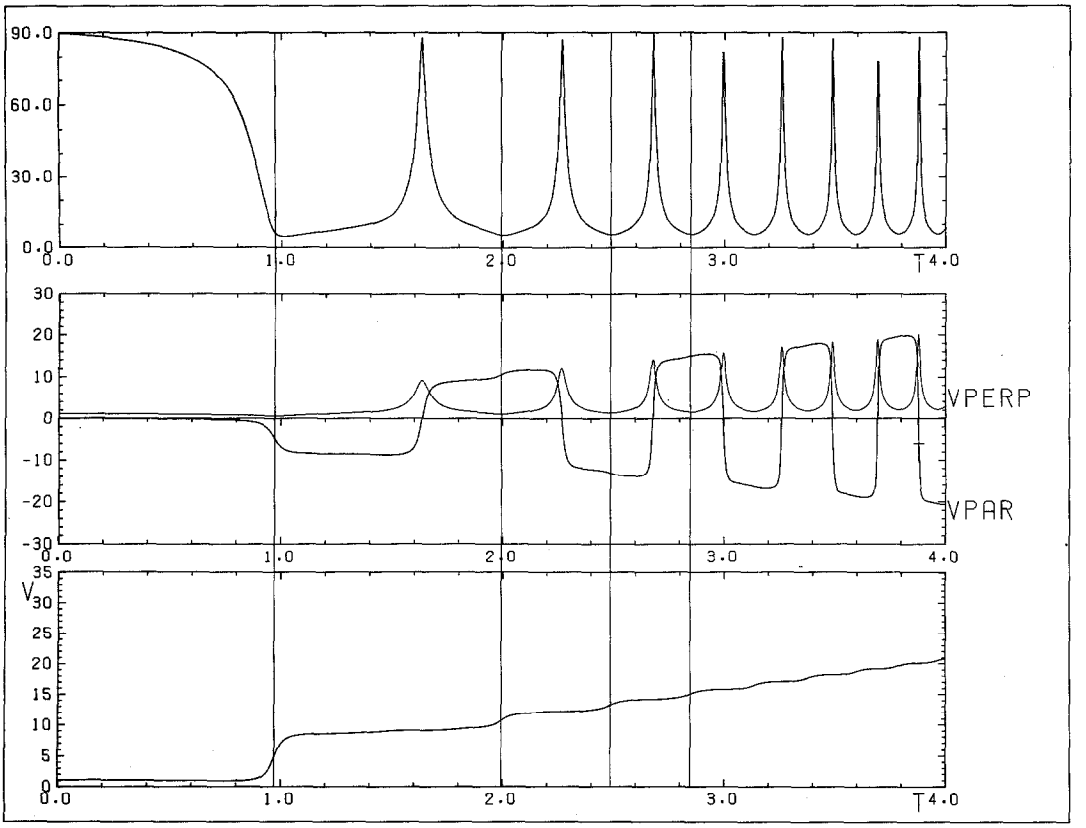

FIG. 1. THE UPPER PANEL SHOWS THE GUIDING CENTRE TRAJECTORY OF AN ION (SOLID LINE) IN THE MODEL FIELD PROJECTED ONTO THE x–z PLANE.

Distances are given as multiples of the plasma sheet scale thickness $k^{-1} \simeq 3.82\ R_E$. The ion was created at the current sheet edge ($z = 6\ R_E$, $z^* \simeq 1.57$) at a downtail distance of $20\ R_E$ ($x^* = -5.24$). The dashed lines denote field lines (contours of constant vector potential). In the lower panel the variation of pitch angle, velocity components and total speed are plotted vs time. Time is expressed in the characteristic units described in section 1, which, for typical field values, is ~ 41 min. The upper plot shows the ion pitch angle defined as $\tan^{-1}(v_\perp/|v_\parallel|)$ which is hence always in the range $0-90°$. The middle plot shows the ion velocity components expressed in units of the characteristic drift speed, which is typically $10\ \mathrm{km\ s^{-1}}$. The total speed of the ion, in the above typical units, is shown in the lower plot. The first few times when the ion crosses the centre plane are marked by vertical lines for reference.

Closer to the Earth ($x \lesssim p$) the $F(x)$ factor ensures that the line dipole contribution dominates.

Values of the field parameters have been chosen to concur principally with the field observed at the release distance $x = -20\ R_E$ since the behaviour of the test particles is found to be sensitively dependent on conditions during the first interaction with the centre of the current sheet. The important properties of the resulting model field are shown in Figs. 1 and 2 of Paper 1, but we will briefly reiterate the field magnitudes at the release distance here for later reference. At $x = -20\ R_E$, the model gives a B_z component which is approximately constant over the plasma sheet thickness (since it is dominated by the dipole term), falling from $\simeq 4$ nT at the centre plane to ~ 3 nT at the sheet edge. The B_x component (dominated by the tail term) varies approximately sinusoidally, from zero at the centre plane to $\simeq 18.1$ nT at the sheet edge ($z = 6\ R_E$). These values are in good agreement with typical quiet time field data (e.g. Behannon, 1968, 1970; Mihalov *et al.*, 1968; Fairfield, 1979).

Another important feature of the model is the uniform, crosstail electric field E_y. Ranges of E_y for which this study is valid will be discussed in Section 4.

We shall now state the simplified guiding centre equations of motion appropriate to this field model. A

more complete discussion may be found in Paper 1, and the equations are given in their general form by, e.g. Northrop (1963).

In a two-dimensional static field with $\mathbf{E}\cdot\mathbf{B}=0$, the motion of the guiding centre may be divided into two parts. The first is the zero order motion in the x–z plane:

$$\frac{\mathrm{d}\mathbf{r}}{\mathrm{d}t}=\mathbf{U}_E+v_{\|}\hat{b} \tag{4}$$

where $\mathbf{U}_E$ is the $\mathbf{E}\wedge\mathbf{B}/B^2$ drift and $v_{\|}$ is the particle speed along the field given by

$$\frac{\mathrm{d}v_{\|}}{\mathrm{d}t}=-\frac{\mu}{m}\frac{\partial B}{\partial s}\mathbf{U}_E\cdot\frac{\mathrm{d}\hat{b}}{\mathrm{d}t}. \tag{5}$$

In equations (4) and (5) $\hat{b}$ is the unit vector along $\mathbf{B}$, s denotes distance along the field and $\mu=mv_{\perp}^2/2B$ is the magnetic moment. Clearly, the above x–z motion is independent of the particle mass or charge. The second part of the guiding centre motion is the sum of the first order drifts V_D across the field lines in the y direction, given by

$$qv_DE_y=\frac{m}{2}\frac{\mathrm{d}}{\mathrm{d}t}(v_{\perp}^2+v_{\|}^2+U_E^2) \tag{6}$$

which is just such as to give conservation of energy for the zero order motion. Another exact integral of the motion which may be obtained from equation (4) is

$$A_y(t)=A_y(t_0)+(t-t_0)E_y \tag{7}$$

where $A_y(t)$ is the magnitude of A_y at the guiding centre at time t. This expression is used to investigate the accuracy of numerical integration of equations (4) and (5).

Having presented the appropriate guiding centre equations of motion, we can now consider the specific properties of the lithium release ions. An important simplification to the initial conditions may be introduced, since the initial "thermal" ion velocity due to the release chemistry ($\sim$4 km s^{-1}) will generally be quite small compared with local plasma flow speeds

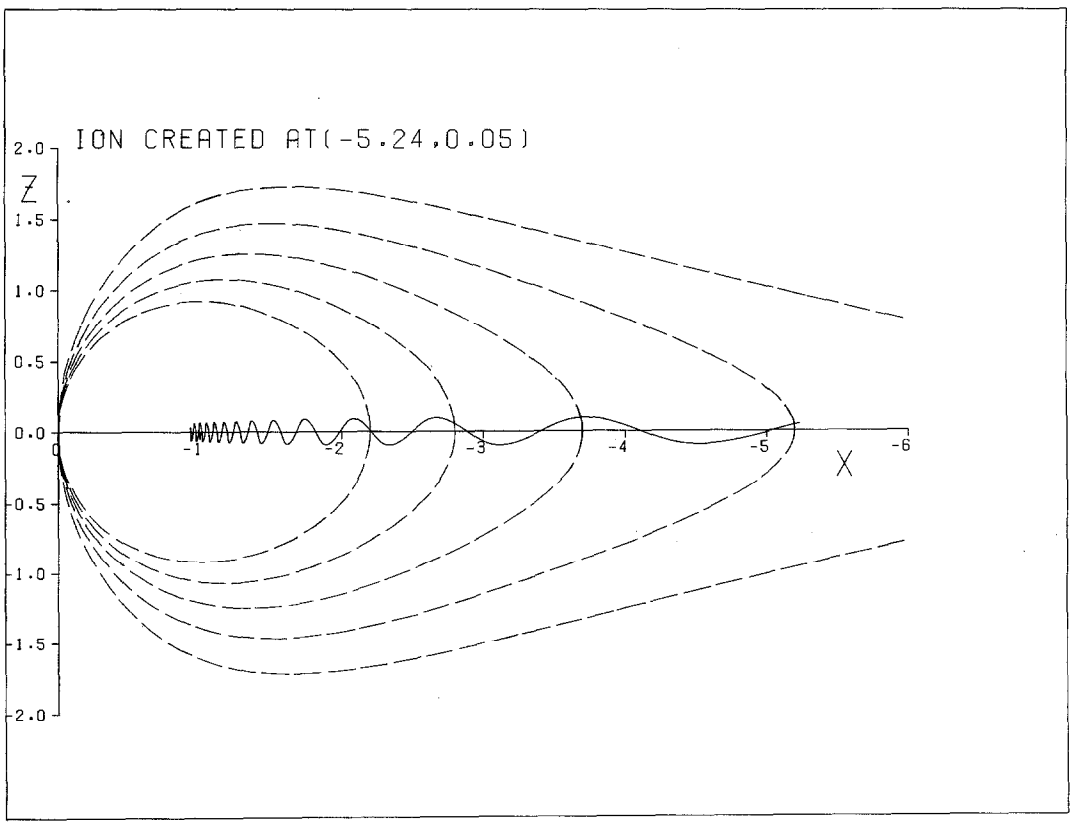

FIG. 2.

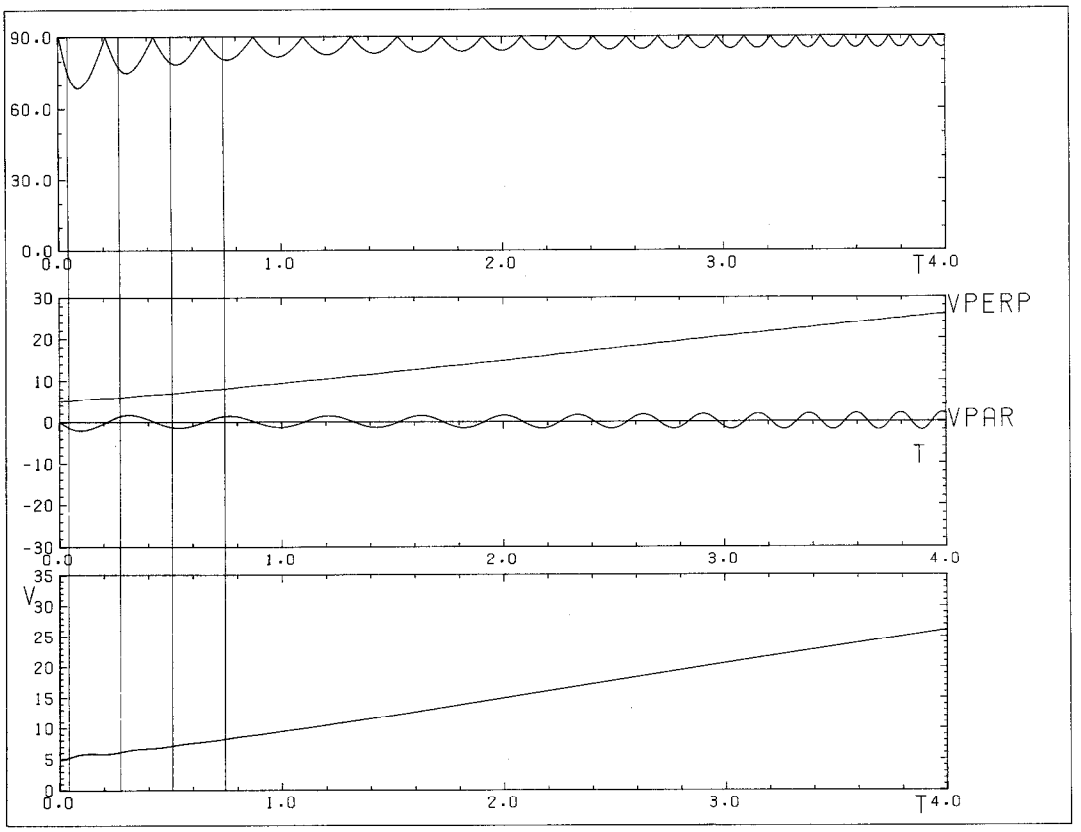

FIG. 2. PLOT OF THE TRAJECTORY, PITCH ANGLE, SPEED AND VELOCITY COMPONENTS IN THE SAME FORMAT AS THE PREVIOUS FIGURE FOR AN ION CREATED AT $z^* = 0.05 (z \simeq 0.19\, R_E)$ AT A DOWNTAIL DISTANCE OF $20\, R_E$, SUCH THAT AT THE POINT OF CREATION $|B_x|/B_z \simeq 0.23$.

(typically ranging from ~ 10 to 50 km s^{-1} over the plasma sheet thickness). A reasonable approximation is then to take the ions as being created at rest, with initial velocity components $v_{\|} = 0$ and $v_{\perp} = |\mathbf{U}_E| = E_y/B$ in the Earth's frame. It is then easy to show (see Paper 1) that since the initial speed is proportional to $\mathbf{U}_E$, the trajectories starting from a given point specified by equations (4) and (5) will have the same form independent of the electromagnetic field magnitude.

The rate at which these trajectories are traced out will depend on the convection speeds, however, so that velocities may be normalized to some typical electric field drift speed $|\mathbf{U}_{E_0}|$. For convenience we have chosen to normalize speeds to the electric field drift speed at any point in the field where $B = 20$ nT. Then given, for instance, $E_y = 0.2$ mV m^{-1} the unit of speed will be 10 km s^{-1}. Lengths have been normalized to the plasma sheet scale thickness k^{-1} which for our model field is just $12/\pi \simeq 3.82\ R_E$. The unit of time is therefore $(k|\mathbf{U}_{E_0}|)^{-1}$ which for the above values is an interval of ~ 41 min. Henceforth, all normalized quantities will be indicated by an asterisk.

3. NUMERICALLY INTEGRATED ION TRAJECTORIES

This section provides a brief review of the nature of ion motion in our model field, described more fully in Paper 1. In order to illustrate ion behaviour, two sample trajectories in the x–z plane are shown in Figs. 1 and 2. These show the trajectories of ions created respectively at the current sheet edge, and close to the centre plane at a down-tail distance $x = -20\, R_E$. The trajectories were obtained by integrations of equations (4) and (5), using a 4th order Runge–Kutte scheme, such that equation (7) was satisfied to an accuracy better than 1% over the entire trajectory.

The behaviour of the majority of ions, created where

$|B| \gg B_z$ (i.e. over $\sim 7/10$ of the plasma sheet height), will be similar to that shown in Fig. 1. After creation at 90° pitch angle and small energy (~ 6.1 eV using the "typical" units of the previous sections) the ion slowly $\mathbf{E} \wedge \mathbf{B}$ drifts to the weak field region close to the centre plane. After strong acceleration along the field, the ion then emerges from the other side of this region having an increased $v_\parallel$ of approximately twice the field line speed at the centre plane $U_E = E_y/B_z$, corresponding to a "typical" energy increase of ~ 260 eV. This behaviour may be understood (to a reasonable approximation) by transforming to the de Hoffman–Teller (de Hoffman and Teller, 1950) frame as explained in Paper 1 (see also Cowley, 1980). The ion then mirrors near the Earth at a field strength which would be attained at a height of $\sim 3.4\ R_E$ above the surface, given a three-dimensional dipole field. Similar energizations occur on subsequent crossings of the centre plane, but these decrease in magnitude as the field line speed at the centre plane is reduced closer to the Earth. The ion finally reaches the ring current region ($x = -8\ R_E, x^* = -2.1$, at the equator) with an energy of ~ 540 eV given the typical field values, and with an equatorial pitch angle of $\sim 5°$ which has remained small throughout the inward transport. This type of motion remains valid for all ions created with $|B_x|/B_z \gtrsim 2$ ($|z^*| \gtrsim 0.45$) which then arrive at the ring current region with similar energies and small pitch angles, $\lesssim 15°$.

Figure 2 shows the behaviour of an ion created close to the centre plane, where $|B_x| \lesssim B_z$. The ion is again created at 90° pitch angle, but now with much larger energy, "typically" ~ 100 eV, since the initial $v_\perp$ is just $E_y/B_c \simeq E_y/B_z$, the field line speed at the centre plane. There is now no significant increase in $|v_\parallel|$, so that the entire ion motion is confined to a region near the equator, and as the ion moves to stronger field regions the equatorial pitch angle increases. The ion arrives at the ring current region with a "typical" energy of ~ 500 eV, similar to that found for ions at smaller pitch angles. Finally, it may be most clearly seen in Fig. 2 that the ion motion during the first few oscillations about the centre plane, in particular $v_\parallel$ and hence the pitch angle, is not symmetric about each centre plane crossing. This effect is due to the presence of convection speeds that are comparable to the ion speed, and will be discussed in the context of the behaviour of the adiabatic invariants in Section 5.

The above results show that there are two factors which determine ion properties. The first is the nature of the initial ion interaction with the current sheet, dependent on where the ion was created, which produces ions of similar energies but differing pitch angles. The second is the changes which take place in $v_\parallel$ and $v_\perp$ during the subsequent inward transport. In Section 5, approximate conservation of longitudinal invariants of the motion will be used to estimate changes in $v_\parallel$. Changes in $v_\perp$ are obtained from assuming conservation of μ; the validity of this assumption will be investigated in the next section.

4. VALIDITY OF THE GUIDING CENTRE APPROXIMATION

In this section we first derive smallness parameters that may be computed along the numerical trajectories, which indicate how well the guiding centre approximation is satisfied. From simple considerations this approximation would be expected to be most suspect in the weak field region close to the centre plane where the field curvature is largest. Numerical evaluation of the smallness parameters derived here for the trajectories in the two-dimensional field show that this is indeed the case. A simple one-dimensional approximation to the two-dimensional field in the region close to the centre plane is thus used to examine analytically the behaviour of the smallness parameters, in order to determine the one which provides the most significant indicator of the breakdown of the adiabatic approximation. We then investigate how large this parameter may become before pitch angle scattering in the current sheet interaction becomes unacceptably large. To do this we have made a study of full trajectory integrations, specified by the Lorentz force law in the simple one-dimensional field model for this region. The results of this numerical study can then be used to demonstrate clearly the relationship between the amount of pitch angle scattering and the size of the most significant smallness parameter.

The basic condition for adiabatic motion is that the change in the magnetic field vector seen by a particle in time Ω^{-1} (where Ω is the gyrofrequency) is small compared with the average field at the particle. We will derive smallness parameters which, for static fields with all cross-field drifts except $\mathbf{U}_E$ being of first order, basically describe the variation of $\mathbf{B}$ seen by the particle due to the motion along, its drift at right-angles to, and its gyromotion about the field.

Consider a particle which is initially at position $\mathbf{r}_0$, where the field is $\mathbf{B}_0 = \mathbf{B}(\mathbf{r}_0)$. Since, to a first approximation, the field may be taken to be uniform over one gyroperiod, then in the time Ω^{-1} the ion may be taken to move on the surface of a cylinder, of radius $v_\perp/\Omega_0$, and length $v_\parallel/\Omega_0$ ($\Omega_0 = qB_0/m$), centred on the field lines, which drifts a distance U_E/Ω_0 perpendicular to $\mathbf{B}_0$. The changes in the field experienced by the particle in this interval may then be estimated by considering the first order variation of the field components over the surface of this drifting cylinder. If the position of some

point on the cylinder is $\mathbf{r} = \mathbf{r}_0 + \mathbf{L}$, then the field components at $\mathbf{r}$ are given, to first order, by the Taylor expansion

$$B_j(\mathbf{r}_0 + \mathbf{L}) = B_j(\mathbf{r}_0) + (\mathbf{L}\cdot\nabla)B_j(\mathbf{r}_0). \tag{8}$$

We consider separately the variations of the field components due to the motion along, about and across the field lines. Putting $\mathbf{L} = \hat{\mathbf{B}}_0 v_{\|}/\Omega_0$ in equation (8), the change in the jth field component due to motion along the field is given by

$$\delta B_j = \frac{v_{\|}}{\Omega_0}(\hat{\mathbf{B}}_0 \cdot \nabla)B_j(\mathbf{r}_0). \tag{9}$$

Summing vectorially over all field components and dividing by B_0 gives the smallness parameter

$$\varepsilon_{\|} = \frac{|v_{\|}|}{\Omega}\frac{|(\mathbf{B}\cdot\nabla)\mathbf{B}|}{B^2} = \frac{|v_{\|}|}{\Omega R} \tag{10}$$

where R is the radius of curvature of the field lines.

To find the maximum variation of B_j due to gyromotion perpendicular to the field, we take $\mathbf{L}$ to be of length $v_{\perp}/\Omega_0$ and to be directed along the component of ∇B_j which is perpendicular to $\mathbf{B}_0$, that is:

$$\mathbf{L} = \frac{v_{\perp}}{\Omega_0}\frac{\hat{\mathbf{B}}_0 \wedge (\hat{\nabla}B_j \wedge \hat{\mathbf{B}}_0)}{\sin\theta} \tag{11}$$

where θ is the angle between $\hat{\mathbf{B}}_0$ and $\hat{\nabla}B_j$. Substitution into equation (8) gives

$$\delta B_j = \frac{v_{\perp}}{\Omega_0}|\hat{\mathbf{B}}_0 \wedge \nabla B_j|. \tag{12}$$

Summing algebraically over all components and dividing by B_0 then gives a second smallness parameter associated with the gyromotion perpendicular to the field:

$$\varepsilon_{\perp} = \frac{v_{\perp}}{\Omega}\sum_j \frac{|\mathbf{B} \wedge \nabla B_j|}{B^2}. \tag{13}$$

Finally to estimate the variation of B_j due to convection across the field, we take $\mathbf{L} = \mathbf{U}_E/\Omega_0$ which from equation (8) gives

$$\delta B_j = \frac{(\mathbf{E} \wedge \mathbf{B}_0)}{\Omega_0 B_0^2}\cdot\nabla B_j. \tag{14}$$

Again summing algebraically over all components and dividing by B_0 then gives a third parameter associated with convection:

$$\varepsilon_d = \sum_j \frac{(\mathbf{E} \wedge \mathbf{B})}{\Omega B^3}\cdot\nabla B_j. \tag{15}$$

From the form of equations (10), (13) and (15) we would expect ε_d only to be of significance in monitoring the validity of the adiabatic approximation during the first interaction with the current sheet, since after this time either $v_{\|}$ or $v_{\perp}$ will always exceed U_E in magnitude. Numerical calculation of the smallness parameters along trajectories in the two-dimensional field show that even in this first interaction $\varepsilon_{\perp} \gtrsim \varepsilon_d$ for ions created close to the centre plane where $v_{\perp}$ is the dominant velocity component, and that the maximum value of ε_d is always less than the maximum in $\varepsilon_{\|}$ for ions created in the strong field region, where $v_{\|}$ ultimately dominates. It is therefore sufficient for our purposes to neglect the effect of electric field drift on the validity of the guiding centre approximation.

The question now arises as to how large $\varepsilon_{\|}$ and $\varepsilon_{\perp}$ may become before pitch angle scattering in the current sheet interaction renders guiding centre theory invalid. In order to investigate this we have integrated the full equation of motion of particles moving in a magnetic current sheet field. For most particles, the important field gradients which lead to non adiabatic behaviour are those in the $\hat{\mathbf{z}}$ direction perpendicular to the equatorial plane. We have therefore used a simple, one-dimensional magnetic field $\mathbf{B} = (B_x(z), 0, B_z)$, where B_z is constant, for the study. B_z may be taken to be constant since we have seen in Section 2 that it is very nearly so over most of the plasma sheet height. The only particles for which this field is inappropriate are those remaining very close to the centre plane, with equatorial pitch angles approaching 90°, for which the weak field gradients in the x-direction present in a two-dimensional field are also important.

As indicated above, numerical calculations of these smallness parameters confirm that the guiding centre approximation is most suspect in the region close to the centre plane. To investigate the breakdown of the theory we therefore need only model the central region of the current sheet, where in general B_x will vary linearly with z to lowest order (see also Fig. 1 of Paper 1). Quite generally, therefore, for the purposes of this study the field may be taken to be given by

$$\mathbf{B}(z) = \left(\frac{B_{x_0} z}{h}, 0, B_z\right) \tag{16}$$

where $B_x = B_{x_0}$ at $z = h$. Also, since B_z is constant, any cross-tail electric field E_y may be removed by transforming to a frame moving in the $+\hat{\mathbf{x}}$ direction with speed $v_T = E_y/B_z$ (Speiser, 1965). We therefore work in the transformed (de Hoffman–Teller) frame where the particle speed will be constant.

An important property of the field given by equation (16), which is convenient for our study, is that since B_x varies linearly with z there is no unique scale length of field variation in the z direction. We can then normalize

distances to length l given by

$$l = \left(\frac{B_z}{B_{x_0}}\right) h \tag{17}$$

such that the normalized distance from the current sheet centre is just equal to the ratio of the B_x and B_z fields at that distance, i.e. $B_x(z^*)/B_z = z^* = z/l$. If times are then normalized to the inverse of the gyrofrequency associated with the field B_z, i.e. to the timescale

$$\tau = \frac{m}{qB_z} \tag{18}$$

the normalized equation of motion becomes

$$\frac{d\mathbf{v}^*}{dt^*} = \mathbf{v}^* \wedge (z^*\hat{\mathbf{x}} + \hat{\mathbf{z}}). \tag{19}$$

This equation contains no reference to the field scale length, since this has, in effect, already been specified by the initial choice of z^* at the start of the trajectory. A particle trajectory in this field may thus be uniquely specified by three independent parameters, namely the particle velocity components, or alternatively the speed, pitch angle and gyrophase, at some arbitrary point (chosen to lie within the mirror points of the trajectory).

This conclusion is implied in the results of a related numerical study by Gray and Lee (1982), who found that changes in the magnetic moment μ are dependent on three parameters, namely the radius of curvature of the field, and the pitch angle and the gyrophase at some reference point in the field. However, this result could not be shown explicitly as here, since the chosen field for their study, $\mathbf{B} = (B_{x_0} \tanh(z/l), 0, B_z)$ has a unique scale length l in the z direction which leads immediately to the inclusion of an extra parameter in the particle equations of motion.

Before discussing the results of the numerical integration, we will first analytically examine the behaviour of the smallness parameters $\varepsilon_\parallel$ and $\varepsilon_\perp$ along an adiabatic trajectory in our one-dimensional model for the field. The result of this analysis will give an indication of which of the smallness parameters is the most important indicator of how well the adiabatic approximation is satisfied.

We can first express $\varepsilon_\parallel$ and $\varepsilon_\perp$ in terms of normalized parameters, and substituting for the one-dimensional field we have

$$\varepsilon_\parallel = \left|\frac{v_\parallel^*}{(z^{*2}+1)^{3/2}}\right| \text{ and } \varepsilon_\perp = \left|\frac{v_\perp^* z^*}{(z^{*2}+1)^{3/2}}\right|. \tag{20}$$

Then since we are working in the de Hoffman–Teller frame, conservation of μ and total speed v^* can be used to relate $v_\perp^*$ and $v_\parallel^*$ to the equatorial pitch angle α_0. Then $\varepsilon_\parallel$ and $\varepsilon_\perp$ as a function of z^* along a trajectory become

$$\varepsilon_\parallel = \left|\frac{v^*(1-(z^{*2}+1)^{1/2}\sin^2\alpha_0)^{1/2}}{(z^{*2}+1)^{3/2}}\right|$$

and

$$\varepsilon_\perp = \left|\frac{v^* z^* \sin\alpha_0}{(z^{*2}+1)^{5/4}}\right|. \tag{21}$$

Clearly $\varepsilon_\parallel$ maximizes at $z^* = 0$, where $v_\parallel$ is maximum and the field radius of curvature is minimum (cf. equation (10)), so that the maximum value of $\varepsilon_\parallel$ in normalized units is just

$$\varepsilon_{\parallel\max} = v^* \cos\alpha_0 = v_{\parallel 0}^*. \tag{22}$$

Examination of the variation of $\varepsilon_\perp$ with z^* also shows that $\varepsilon_{\parallel\max} > \varepsilon_{\perp\max}$ for $\alpha_0 \lesssim 67.8°$, and for larger equatorial pitch angles $\varepsilon_\perp$ maximizes at the mirror points, giving

$$\varepsilon_{\perp\max} = v^* \sin^4\alpha_0 \cos\alpha_0 (1+\sin^2\alpha_0)^{1/2} \geqslant \varepsilon_{\parallel\max}. \tag{23}$$

If the maximum allowed value of either parameter for the particle behaviour to be adiabatic is then some constant $\varepsilon_{\max} \leqslant 1$, then the maximum allowed speed $v_{\max}^*$ as a function of equatorial pitch angle is given by

$$v_{\max}^* = \frac{\varepsilon_{\max}}{\cos\alpha_0} \quad \text{for } \alpha_0 \lesssim 67.8° \tag{24}$$

$$v_{\max}^* = \frac{\varepsilon_{\max}}{\cos\alpha_0 \sin^4\alpha_0 (1+\sin^2\alpha_0)^{1/2}} \quad \text{for } \alpha_0 \gtrsim 67.8°.$$

The maximum speed is thus equal to $\varepsilon_{\max}$ for field-aligned particles, increasing to infinity with increasing pitch angle. Thus 90° pitch angle particles are adiabatic in this field at all energies, as expected, since they simply experience the constant field B_z at $z^* = 0$. The effect of the weak field variations in the x direction must then in general be considered for large pitch angle particles, and since it can be shown that this will not significantly affect the above conclusion that guiding centre theory will first be violated by small pitch angle particles as they cross the centre plane, it is sufficient to discuss this briefly later. Here we will now consider the results of the numerical integration of equation (19) in the one-dimensional field.

A more extensive study of this nature has been given by Gray and Lee (1982), which yields similar results to those presented here. However, we have seen that the field model used in their study does not have the special properties which allow particle motion to be parameterized as simply as has been described in this section. This parameterization will allow the conditions required for the validity of the guiding centre

approximation to be assessed in a more straightforward way than given by Gray and Lee (1982), since the size of the most important smallness parameter $\varepsilon_{\parallel_{max}}$ can be directly related to the particle speed from equation (22).

The particle equation of motion (19) has been integrated using a fourth order Runge–Kutte scheme. The accuracy of the integration was verified by simultaneously calculating two constants of the motion, energy and canonical momentum in the y direction. The time step was chosen to be velocity dependent ($\Delta t = 1/(100\sqrt{v^*})$ such that the change in the constants of the motion over each trajectory was less than $\sim 10^{-2}\%$. Particles were started at a z^* value where their behaviour was expected to be adiabatic, with velocity coordinates such that if they remained adiabatic they would cross the equator with pitch angle α_0 and field-aligned speed $v^*_{\parallel_0}$.

The behaviour of a particle in the field reversal region is easily visualized with reference to a diagram of the particle equatorial pitch angle α_0 vs height above the centre plane z^* for all points along the trajectory. The instantaneous α_0 is obtained from the instantaneous local pitch angle α (where $\alpha = \cos^{-1}(\mathbf{v}^* \cdot \mathbf{B}^*)$) by conservation of μ. An example of such a plot is shown in Fig. 3, for particles started at various $v^*_{\parallel} = v^*_{\parallel_0}$ that are all initially field-aligned. The trajectories shown were all started at $z^* = 5.5$, where the behaviour is adiabatic, and hence where α_0 is a constant (zero). As the particles approach the centre plane, it can be seen that there is a

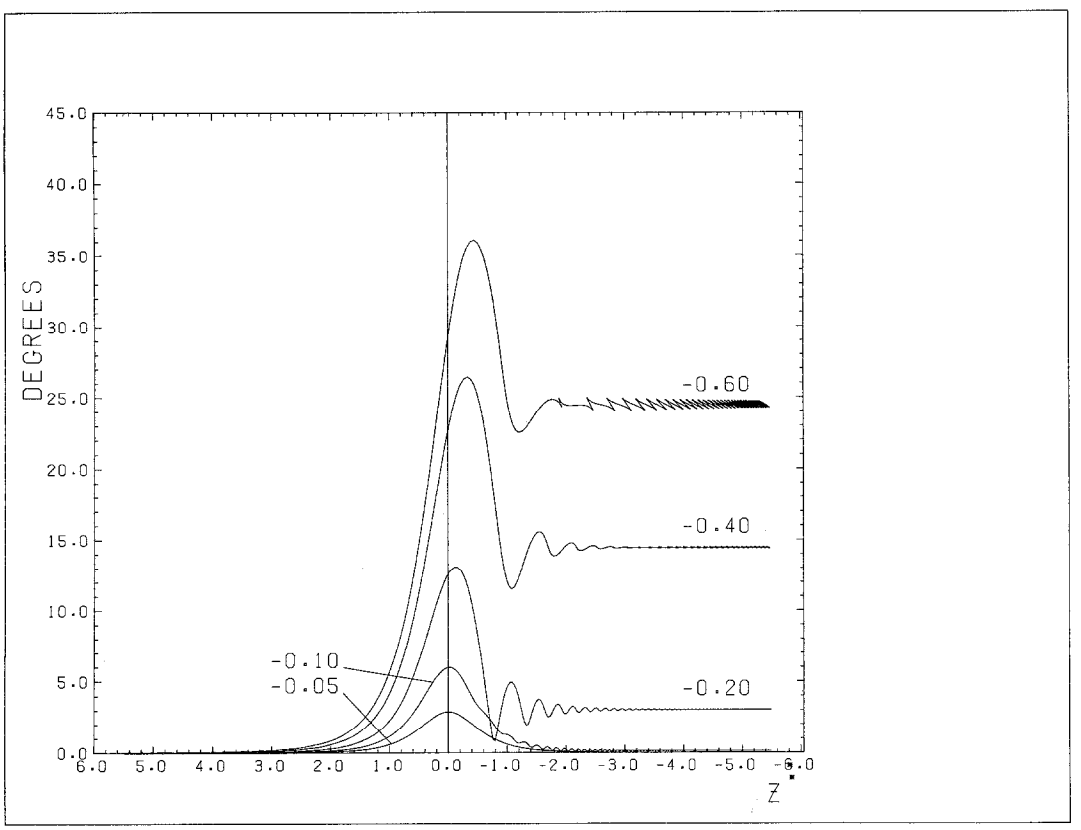

FIG. 3. PLOT OF THE EQUATORIAL PITCH ANGLE α_0 VS THE NORMALIZED DISTANCE FROM THE CENTRE PLANE z^*, FOR EXACT PARTICLE MOTION IN THE ONE-DIMENSIONAL ($E = 0$) FIELD.
Since this field has no unique scale length, distances are normalized with respect to the x and z field components at the particle position, such that $z^* = B_x(z)/B_z$. The equatorial pitch angle is obtained from the particle velocity components at any given z^* by conservation of μ. The curves shown correspond to the trajectories of the particles that were initially field aligned; the initial normalized velocities along the field are also given. The normalized units of velocity are such that these initial equatorial parallel velocities are just given by the magnitude of the smallness parameter, $\varepsilon_{\parallel_{max}}$, appropriate to the trajectory.

large increase in α_0. This is essentially due to the cross-field (y-direction) curvature drift in the current sheet field, which increases the component of the local particle $\mathbf{v}^*$ in the y direction, and hence $\cos^{-1}(\mathbf{v}^* \cdot \mathbf{B}^*)$. For adiabatic particles, such as the trajectory shown with $v^*_{\parallel 0} = 0.05$, the curves are, of course, symmetrical about $z^* = 0$, so that on the other side of the current sheet α_0 again falls to zero. However, as the particle speed is increased, we see that the curves are no longer symmetrical, and that the particles emerge on the other side of the current sheet with successively larger equatorial pitch angles. As the particles move to regions of larger $|z^*|$, where behaviour is once again adiabatic, the equatorial pitch angles again approach constant values. The small oscillations in α_0 in what is clearly a region of adiabatic behaviour (i.e. $|z^*| > 3.0$) are due to finite Larmor radius effects, since α_0 has been calculated at the particle, rather than at the guiding centre position.

Results such as those shown in Fig. 3 for initial $\alpha_0 = 0$ were obtained for a range of initial equatorial pitch angles and gyrophase. In Fig. 4 we have plotted the change in α_0 on crossing the centre plane vs the value of $v^*_{\parallel 0}$ at the start of the trajectory, for particles at various initial α_0 and at arbitrary gyrophase. We have also only given results for particles with initial pitch angles $\alpha_0 \leqslant 45°$, since it has already been shown that the guiding centre approximation will first be violated for small pitch angle particles in the weak field region.

Since ions created in the lithium release in the tail may reach the weak field region (where the guiding centre approximation will first be violated) with any

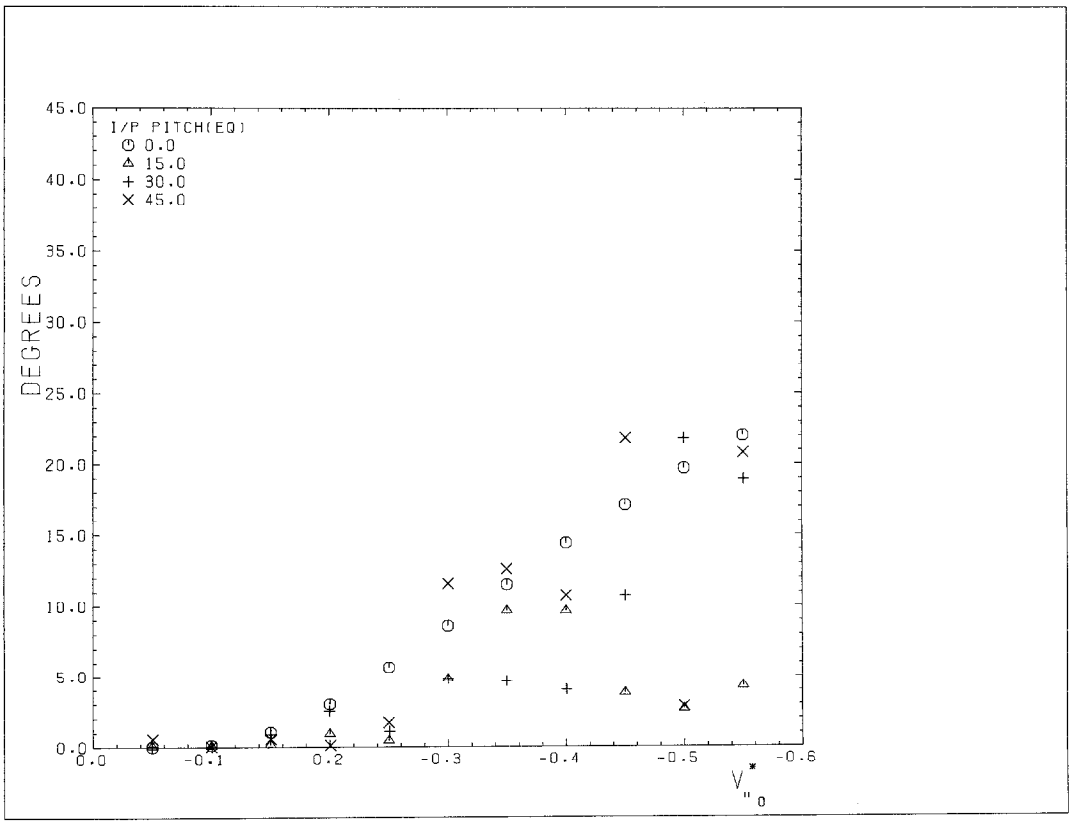

FIG. 4. THE MAGNITUDE OF THE CHANGE IN THE EQUATORIAL PITCH ANGLES OF PARTICLES OVER ONE CROSSING OF THE CENTRE PLANE IS PLOTTED VS THE NORMALIZED INITIAL EQUATORIAL FIELD-ALIGNED VELOCITY.
The results shown are for exact particle motion in the one-dimensional ($E = 0$) field. Different symbols indicate the initial equatorial pitch angles of the particles, as shown in the top left of the plot. The normalization of velocity has the same significance as in the previous figure. An arbitrary value was assigned to the initial gyrophase.

possible gyrophase, we need only be aware here of the maximum possible pitch angle scattering for an ion of given speed and pitch angle. Hence we will not discuss in detail results of the dependence of pitch angle scattering on initial gyrophase (which may also be found in Gray and Lee, 1982), but will instead state the results from Fig. 4 that the maximum possible pitch angle change for particles which initially have $\alpha_0 \neq 0$ is similar to or smaller than that found for $\alpha_0 = 0$ particles, which of course is independent of gyrophase considerations. Looking now at Fig. 4, we see that some scatter, due to the arbitrary choice of gyrophase, is evident, but various regimes of behaviour are clear. Firstly, if the initial $v^*_{\|0} < 0.15$, then pitch angle scattering is clearly negligible. As the initial $v^*_{\|0}$ is increased above this limit, some pitch angle scattering is evident, but provided that $v^*_{\|0} < 0.25$ initially this scattering is acceptably small, that is <5–$10°$. Beyond this limit, however, it can be seen that the amount of scattering becomes progressively larger.

We have seen in Section 2 that, under the particular conditions of an AMPTE tail release, the guiding centre trajectories of lithium ions are found to be independent of the electromagnetic field magnitudes, and hence that velocities may be normalized with respect to these magnitudes. In particular, the characteristic velocity to which all other velocities may be normalized is proportional to the cross-tail electric field strength. Therefore, in determining any limitations on the value of $v^*_{\|0}$, and hence v^*, we are essentially specifying an upper limit on E_y for which ion motion in a given tail field will be adiabatic. Now we have seen from equation (22) that limits on $v^*_{\|0}$ correspond to limits on $\varepsilon_\|$, written in normalized form. Using equation (10) to obtain an expression for $\varepsilon_\|$ in terms of the two-dimensional field at the centre plane (where pitch angle scattering will first occur) we have

$$\varepsilon_{\|\max} = \frac{v_{\|0}}{\Omega_z} \cdot \frac{1}{B_z} \frac{\mathrm{d}B_x}{\mathrm{d}z}\bigg|_{z=0} . \tag{25}$$

This parameter will maximize as the ions first cross the centre plane, since it is here that the field radius of curvature is smallest, so that we may put $v_{\|0} \approx E_y/B_z$ in equation (25). Using the typical quiet time field magnitudes of our model at the release distance $x = -20\ R_E$, $z = 0$ (where $B_z = 3.9$ nT, $\mathrm{d}B_x/\mathrm{d}z \simeq 4.6$ nT R_E^{-1}) in equation (25), the above limits on $v^*_{\|0}$, and hence $\varepsilon_\|$ for negligible and moderate pitch angle scattering then translate to upper limits on cross-tail electric fields of ~ 0.2 mV m^{-1} and ~ 0.3 mV m^{-1} respectively.

However, since the ions first cross the centre plane earthwards of the release distance, where the field radius of curvature is larger, the above values represent an underestimate of the upper limits on E_y for minimal pitch angle scattering. If, instead of the purely analytical estimate above, we use the numerically computed trajectories to determine the point where the ions first cross the centre plane and then use the field values at that point to calculate the limits on E_y, more realistic values of approximately ~ 0.2 mV m^{-1} and ~ 0.4 mV m^{-1} respectively are obtained for small pitch angle ions.

In addition to the above upper limits on E_y, a lower limit on E_y is also imposed by the assumption that the initial "thermal" speed of the ions may be neglected compared to the electric field drift speeds in the tail. A brief discussion of this point, which may be found in Paper 1, shows that the resulting lower limit is $E_y \gtrsim 0.04$ mV m^{-1}. Summarizing, then, the assumptions of our model should be valid over the electric field range $0.04 \lesssim E_y \lesssim 0.4$ mV m^{-1}, which clearly spans the range of usual quiet time values. Typically $E_y \simeq 0.2$ mV m^{-1}, corresponding to a cross-tail potential of 50 kV (e.g. Reiff *et al.*, 1981).

To complete this study on the conditions which lead to non-adiabatic behaviour, we shall finally briefly discuss the effect of the weak gradients in the x-direction on the validity of the guiding centre approximation for large pitch angle particles. Values of the smallness parameters have been calculated numerically along the trajectories of ions in the two-dimensional field model. In this field we would then expect $\varepsilon_\perp$ to tend to some finite value (rather than zero as in the one-dimensional model studied in this section) as the ion equatorial pitch angle approaches 90° and $\varepsilon_\|$ goes to zero, and this is found to be the case. For instance, given the typical magnetic field magnitudes from Section 1, and $E_y = 0.2$ mV m^{-1} for a lithium ion created very close to the centre plane at $z^* = 0.01$, with a minimum pitch angle of $\sim 86°$, the maximum $\varepsilon_\perp$ is 0.0216 during the first current sheet interaction, compared to the maximum $\varepsilon_\|$ of 0.012. The ion created at the centre plane with 90° pitch angle, and hence $\varepsilon_\| = 0$, is created with $\varepsilon_\perp = 0.012$, which increases to $\simeq 0.017$ in the ring current region. However, it is also expected that, since the field gradients in the z direction are much larger than those in the x direction in the region where ions first interact with the current sheet, the above maxima in $\varepsilon_\perp$ for large pitch angle particles whose motion is largely perpendicular to the field should be much less significant than the maxima in $\varepsilon_\|$ for small pitch angle particles with motion principally along the field. Since, for the same electromagnetic field magnitudes as above, it is found that for an ion created at the plasma sheet edge, $\varepsilon_\|$ maximizes in the first current sheet interaction with a value $\simeq 0.145$, this is found to be the case. Our assumption that the adiabatic approximation will first be violated by small pitch angle

ions during the first current sheet interaction is therefore valid.

In this section we have demonstrated that the approximations used to produce the trajectories discussed in Section 3 will be valid for lithium ions over the typical range of quiet time values of E_y, for our given two-dimensional magnetotail field. The results given in Fig. 4 (together with similar results presented in a less accessible form by Gray and Lee (1982)) may also be simply used to estimate the amount of pitch angle scattering of ions in any general field reversal region. In the next section, we will show how the numerical results of Section 3 may also be generalized, so that the behaviour of the lithium test ions may be approximately deduced for any given model of the magnetotail.

5. APPROXIMATE LONGITUDINAL INVARIANTS OF THE MOTION

In order to estimate ion properties on arrival in the dipole dominated nightside ring current region, we must first consider analytically the behaviour of ions in their initial interaction with the tail current sheet, before discussing invariants which determine their behaviour during subsequent inward convection towards the Earth.

The ions will all be created uniformly in z between the centre plane and the current sheet edge. For reasons given in the previous section, the two-dimensional field may be approximated by

$$\mathbf{B} = (B_x(z), 0, B_z) \tag{26}$$

over most of this range. Once again, we may transform to a frame where the cross-tail electric field E_y is zero (i.e. the de Hoffman–Teller frame), that is, the field line rest frame, by moving in the $+x$ direction with transformation speed $v_T = E_y/B_z$. The initial velocity coordinates of the newly created ion, in the Earth and de Hoffman–Teller frame, are shown in velocity space in Fig. 5.

In the Earth (unprimed) frame, the ion is created at rest (at point A) so that its guiding centre (at point G) moves with the electric field drift velocity $v_{gc} = v_\perp = E/B_c$. The ion is therefore created with the transformation speed $v = v_T = E_y/B_z$ in the de Hoffman–Teller frame, and with pitch angle α just equal to the angle between the field and the centre plane (x axis), given by $\tan\alpha = B_z/B_x$. Since $v = v_T$ regardless of the distance of the creation point from the centre plane, and as B_z is nearly constant, all the ions will have the same speed in the de Hoffman–Teller frame and hence will all lie on a sphere in velocity space of radius $v_T = E_y/B_z$. The pitch angle with which an ion arrives

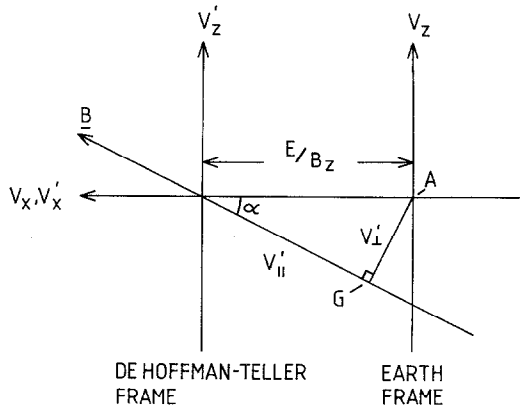

FIG. 5. THE VELOCITY SPACE DIAGRAM SHOWS THE RESULT OF APPLYING A FRAME TRANSFORMATION TO THE INITIAL CONDITIONS OF THE LITHIUM IONS.
Velocity coordinates in the de Hoffman-Teller frame are obtained from those in the Earth frame by moving in the $+x$ direction with speed $v_T = E/B_z$. In the Earth frame, the ions are created at rest at point A, so that the guiding centre at point G moves with $v_\perp = E/B_c$, $v_\parallel = 0$ (where B_c is the field at the creation point). In the de Hoffman–Teller frame, the ion has constant speed $v' = v_T = E/B_z$, and pitch angle α.

at the centre plane, α_0, is just obtained from the pitch angle α at the creation point by conservation of μ, so that

$$\sin^2\alpha_0 = \sin^2\alpha\frac{B_z}{B_c} = \left(\frac{B_z}{B_c}\right)^3. \tag{27}$$

The minimum pitch angle at the centre plane is just that of an ion created at the plasma sheet edge, where the field is strongest. Hence, if $B_x = B_{max} \simeq 18$ nT, and $B_z \simeq 4$ nT, equation (27) gives $\alpha_{0_{min}} \simeq 6°$, which compares favourably with the numerical value found for the trajectory shown in Fig. 1. We have shown then that, in the de Hoffman–Teller frame, all the ions will lie on a sphere in velocity space, given by

$$v'^2_\parallel + v'^2_\perp = (E_y/B_z)^2 \tag{28}$$

at all pitch angles $\alpha_0 \gtrsim 6°$.

Now, since $v_\perp = (\mathbf{v} - \mathbf{U}_E)_\perp = v'_\perp$ and at the centre plane $v'_{\parallel 0} = v_{\parallel 0}$ equations (27) and (28) will also hold for ions in the Earth frame as they cross the centre plane. We can then compare equation (28) with the velocity components of ions obtained from the numerically calculated trajectories in the two-dimensional field as they first intersect the centre plane. These velocity components, in the normalized units given in Section 2, are plotted in velocity space in Fig. 6 for ions created non-uniformly over the current sheet thickness at $x = -20\ R_E$. Also shown by a solid line is a quadrant of a

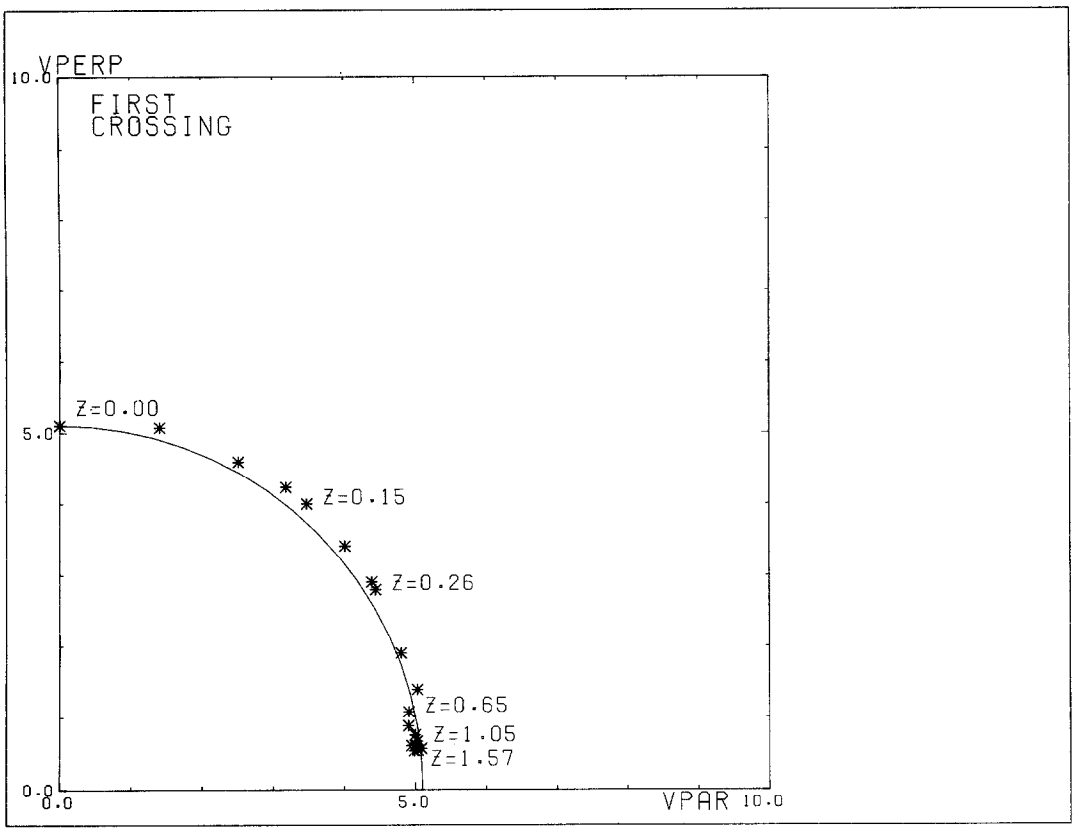

FIG. 6. THE NORMALIZED VELOCITY COMPONENTS OF IONS AS THEY FIRST CROSS THE CENTRE PLANE ARE SHOWN BY THE ASTERISKS IN VELOCITY SPACE.
The ions were created non-uniformly over the current sheet thickness at $x = -20\ R_E$, the distance of the creation point from the centre plane, normalized to the scale thickness $k^{-1} \simeq 3.82\ R_E$, is given for various examples. Velocities are again given in terms of the characteristic units discussed in Section 2, and are typically $\sim 10\,km\,s^{-1}$. The solid line shown is part of a circle with a radius given by the normalized field line speed at the centre plane at $x = -20\ R_E$.

circle of radius $v^* = U^*_{E_0}$, the normalized electric field drift speed at the centre plane at the release distance ($x = -20\ R_E$) in the two-dimensional model, and it is clear that all the ions lie close to this circle. Note that the 90° pitch angle ion lies exactly on the circle since it was created in the centre plane at $x = -20\ R_E$, with $v_\perp = U_{E_0}$ in the Earth frame. In order to illustrate the dependence of equatorial pitch angle on the distance of the creation point from the centre plane, various ions shown in Fig. 6 have been labelled according to creation height z^*. It is then clear that, as suggested by previous statements, if the ions were created uniformly over the thickness of the current sheet, most would appear at small pitch angles after first crossing the centre plane. The small pitch angle ions would then have $v^*_{\|_0} \simeq v^*$ $= E_y/B_z$ as they first cross the centre plane, increasing to twice this value in the Earth frame as the ions reach the strong field region on the other side, as implied by the de Hoffman–Teller frame transformation (see Paper 1).

Having obtained approximate analytical estimates of the velocity components of ions as they first cross the centre plane that are in good agreement with the numerical results for the two-dimensional field, it remains to discuss how $v_\perp$ and $v_\|$ vary during the subsequent inward transport.

Clearly the variation of $v_\perp$ is determined by conservation of μ, provided guiding centre theory is valid. We therefore only need to look in detail at the behaviour of $v_\|$, and whether the variation can be

estimated from a longitudinal invariant related to the second adiabatic invariant

$$J = \oint v_{\parallel}\, ds \tag{29}$$

where ds is the distance along the field. This invariant will, in general, be preserved only if the effects of guiding centre drifts perpendicular to the field, which carry the particle from its original field line, are small on the timescale of the particle oscillation between the mirror points (Northrop and Teller, 1960). This implies that, as well as effective changes in the "potential well" in which the particle oscillates being first order over a bounce period, we require that J is calculated in a frame of reference in which the cross-field speed, in our case the convection speed U_E, is first order. Although our field model is static, it is clear that U_E is not first order in the weak field regions at the creation distance, being instead comparable to the ion speeds in this region. We would therefore not expect J to be well preserved if calculated in the Earth's frame until the ions reach the strong field regions closer to the Earth where U_E is smaller. However, if it is possible to transform to the de Hoffman–Teller frame where $U_E = 0$, it is clear that if changes in the particle "potential well" are small J calculated in this new frame should be conserved.

The effect of zero order convection can be clearly envisaged if we calculate J for a particle moving in a simple one-dimensional field such as that given by equation (26), but in a frame moving in the x direction with constant speed $v_T = E_y/B_z$, where E_y is the electric field in this moving frame. If, in the de Hoffman–Teller frame, where $v_T = 0$

$$J_H = \oint v_{\parallel H}(t)\, ds = \oint v_{\parallel H}^2(t)\, dt \tag{30}$$

then in the moving frame $v_{\parallel}(t) = v_{\parallel H}(t) + \dfrac{B_x}{B} v_T$ and

$$\begin{aligned} J &= \oint v_{\parallel}^2(t)\, dt \\ &= J_H + 2v_T \oint v_{\parallel H}(t) \frac{B_x}{B}\, dt + v_T^2 \oint \left(\frac{B_x}{B}\right)^2 dt \end{aligned} \tag{31}$$

when v_T is small then $J \simeq J_H$ and should clearly be conserved. However, when v_T is not small compared to $v_{\parallel H}$, then two terms appear. The middle term will integrate to zero over a bounce period, provided that v_T and the net $v_{\parallel}$ do not change in this time. The last term, however, will give some finite value proportional to v_T^2, and hence in regions of a trajectory where v_T is large will contribute to the calculated value for J. Hence J will no longer be conserved if v_T changes during the particle transport.

In order to investigate this in more detail we have numerically calculated the values of the following integral along the trajectories in the two-dimensional field:

$$J(\tfrac{1}{4}) = \int_0^{Sm} v_{\parallel}\, ds = \int_0^{Sm} v_{\parallel}^2\, dt \tag{32}$$

where the integrals are taken over successive quarter bounce periods between the equator and a mirror point, or *vice versa*. The numerical uncertainties in the computed $J(\frac{1}{4})$ are $\lesssim 0.05\%$. The results for the majority of ions, created where $|B_x| \gtrsim B_z$ are shown in Fig. 7, where the integrals $J^*(\frac{1}{4})$, normalized according to the typical units of sections 2 and 3, are plotted vs the "bounce number". Each "bounce number" refers to the section of the trajectory that lies between two successive mirror points, which hence contains two quarter-bounce intervals. Thus, for instance, the part of the trajectory which lies between the creation point and the first mirror point is denoted by bounce number 1. The results have been computed for the first ten bounce numbers, which represents ion motion that has continued to well within the ring current region (e.g. see Figs. 1 and 2.)

After an initial rapid increase due to the large acceleration along the field as the ion first crosses the centre plane, the values of $J^*(\frac{1}{4})$ appear to oscillate about some constant average. Larger values of $J^*(\frac{1}{4})$ occur on alternate bounce periods which correspond to time when the ion is moving towards the Earth, and has just been accelerated along the field after crossing the centre plane. It is clear therefore that this oscillation in $J^*(\frac{1}{4})$ is essentially due to the presence of convection (which results in this acceleration along the field), and corresponds to the second term on the right-hand side of equation (31). We would then expect this effect to average approximately to zero on the two halves of a trajectory from the mirror point to the equator and back to the mirror point again. The result of taking such an average is shown in Fig. 8, where successive values of $J^*(\frac{1}{4})$ have been added to give a single value $J^*(\frac{1}{2})$ appropriate to each bounce number.

It can be seen in Fig. 8 that, after the ions first mirror close to the Earth, $J^*(\frac{1}{2})$ is well preserved. However, ions created near the edge of the current sheet, where the initial $|B_x|/B_z$ ratio is large (as given on the R.H.S. of the diagram) have a value of $J^*(\frac{1}{2})$ that is smaller in the first than in subsequent bounces, the change being $\sim 28\%$ of the final value. This effect is due mainly to large changes in the path length of the ion trajectory between the first and second half bounce periods (see Fig. 1), but a contribution due to large convection speeds, as suggested by the last term in equation (31), which would change in magnitude as U_E decreases between subsequent half bounce periods, would also be present. The change in $J^*(\frac{1}{2})$ is reduced for ions starting closer to

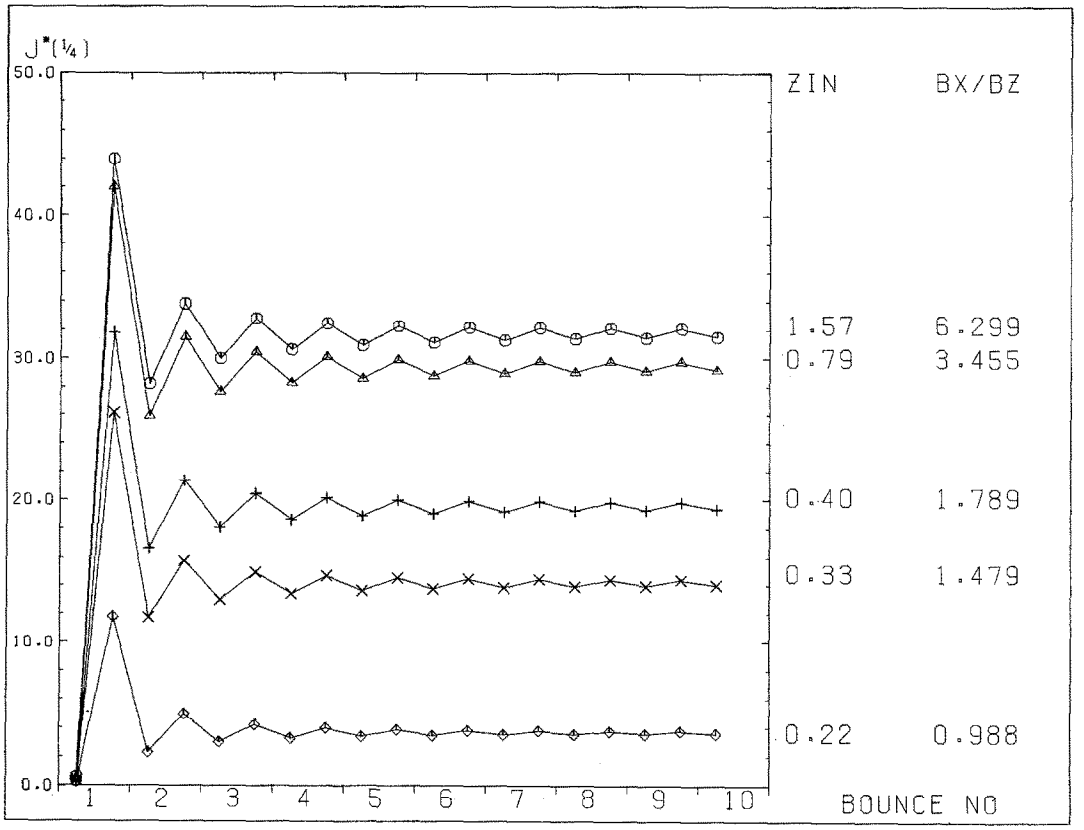

FIG. 7. THE NORMALIZED SECOND ADIABATIC INVARIANT, CALCULATED OVER SUCCESSIVE $\frac{1}{4}$-BOUNCE PERIODS, $J^*(\frac{1}{4})$, IS SHOWN PLOTTED AGAINST "BOUNCE NUMBER", FOR GUIDING CENTRE TRAJECTORIES CALCULATED IN THE TWO-DIMENSIONAL MODEL FIELD.

$J^*(\frac{1}{4})$ is expressed in terms of the characteristic units of velocity given in Section 2, and the scale thickness k^{-1}, which for typical field magnitudes translates to units of $\sim 2.4 \times 10^5$ km^2 s^{-1}, and bounce numbers refer to the sections of trajectories which lie between successive mirror points. The distance from the centre plane at which the ions are created, also normalized to the scale thickness k^{-1}, is given on the right hand side of the plot, along with the $|B_x|/B_z$ ratio at the creation point.

the current sheet centre, as the path length change decreases, and reverses in sense for initial $|B_x|/B_z \lesssim 1$, as the change in $J^*(\frac{1}{2})$ due to convection alone dominates. The final constant values of $J^*(\frac{1}{2})$ also decrease with decreasing initial distance from the sheet centre. Although we have seen in Section 3 that all ions created where $|B_x| \gtrsim B_z$ are accelerated to similar parallel speeds on first crossing the centre plane, ions created close to the current sheet centre have successively larger μ and thus mirror further from the Earth. This results in a reduced path length between mirror points and hence a reduced value of J^*.

These results indicate that useful estimates of the variation of $v_\parallel$ during inward transport may be obtained from conservation of J. However, J itself is not a convenient parameter to employ directly, and must be further approximated for simple use. For ions created near the current sheet edge whose equatorial pitch angles are small, a simple approximation is

$$J(\tfrac{1}{2}) \simeq I(\tfrac{1}{2}) = v_{\parallel_0} L \tag{33}$$

where $v_{\parallel_0}$ is the field-aligned speed of an ion as it crosses the equator and L is the total length of the field line passing through that point (from the Earth to the equator and back). It should be noted from Fig. 1 that $v_{\parallel_0}$ will represent a value of $v_\parallel$ which is intermediate between the nearly constant values prior to, and after a current sheet interaction, as required. The expression for $I(\frac{1}{2})$ represents a good estimate of $J(\frac{1}{2})$ even for the first bounce interval from the point of creation to the

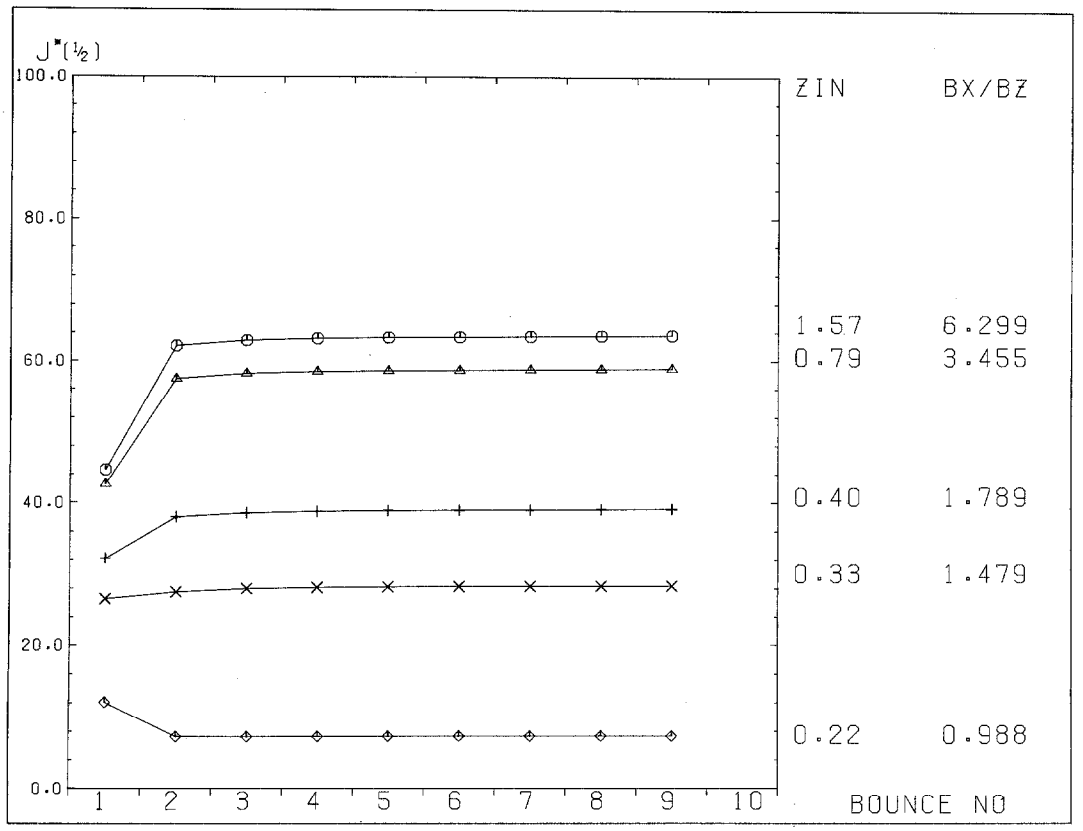

FIG. 8. THE NORMALIZED SECOND ADIABATIC INVARIANT, CALCULATED AFTER SUCCESSIVE $\frac{1}{2}$-BOUNCE PERIODS, $J^*(\frac{1}{2})$, IS SHOWN FOR THE SAME ION TRAJECTORIES AND IN THE SAME FORMAT AS THE PREVIOUS FIGURE. $J^*(\frac{1}{2})$ is obtained by simply adding the successive pairs of $J^*(\frac{1}{4})$ values corresponding to each bounce number.

mirror point. The contribution of first quarter bounce to the first $J(\frac{1}{2})$ value can be seen from Fig. 7 to be negligible (since $v_{\|} \approx 0$ until the ions are very close to the centre plane) while the contribution of the second quarter bounce is approximately twice $v_{\|_0}$ (e.g. see Fig. 1) times half the total field line length at the equatorial crossing. Therefore we expect $I(\frac{1}{2})$ to be an approximate invariant during the inward motion of small pitch angle ions from the first crossing onwards. A good approximation to the latter value is already known from the results given earlier in this section.

The degree to which $I(\frac{1}{2})$ is invariant for our computed trajectories is shown in Fig. 9, where we plot $v^*_{\|_0}L^*$ for successive crossings of the centre plane.

The curves show similar behaviour to those of $J^*(\frac{1}{2})$ in Fig. 8, but are systematically higher in value since the total field line length L is generally an overestimate of the ion path length along the field between the mirror points, and increasingly so for particles created successively closer to the centre plane. The results in Fig. 9 do show, however, that approximate conservation of $I(\frac{1}{2}) = v_{\|_0}L$ can be used to estimate the variation of $v_{\|_0}$ during inward transport, at least for ions created at distances $z^* \gtrsim 0.33$ where $|B_x|/B_z \gtrsim 1.5$. The largest errors in this range due to the change in $J(\frac{1}{2})$ between the first and second bounce number range are $\simeq 17\%$. The invariant becomes less satisfactory, however, at $z^* \simeq 0.22$ and below, where $B_x/B_z \lesssim 1$.

This then gives an estimate of the range of values of creation height for which this approximate invariant may be taken to be valid in a two-dimensional field. To extend this result to the three-dimensional case, it seems reasonable that the approximate invariant will be useful for all ions which traverse more than half the field line length between the equator and the Earth's centre on their first half period of oscillation. This is just the situation which occurs for the ion created at $|z^*| = 0.22$ in the two-dimensional field. Therefore in the AMPTE

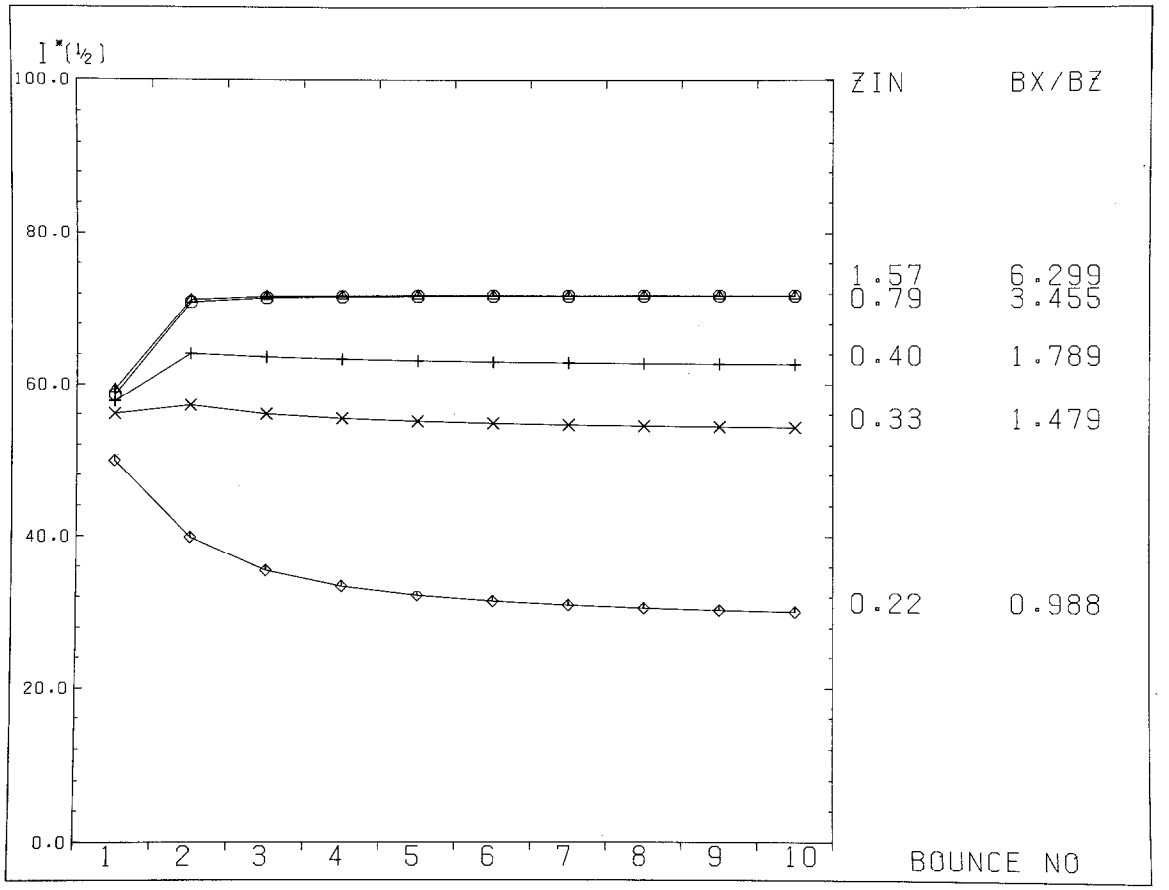

FIG. 9. THE APPROXIMATE LONGITUDINAL INVARIANT $I^*(\frac{1}{2}) = v^*_{\|_0} L^*$ HAS BEEN CALCULATED FOR THE TRAJECTORIES REFERRED TO IN THE PREVIOUS FIGURE, AND IS PLOTTED IN THE SAME NORMALIZED UNITS AND FORMAT.
Curves appertaining to the same trajectories are plotted with the same symbols, for comparison.

lithium experiment, all ions that may reasonably be expected to conserve $v_{\|_0} L$ must mirror within $\sim 10\ R_E$ of the Earth, since the ion release will take place $\sim 20\ R_E$ downtail. If the Earth's field is then taken to be approximately dipolar, so that the field strength at $10\ R_E$ is $\sim$ 50 nT, while the field at the centre plane at $20\ R_E$ is $\sim$ 4 nT, then such ions must have pitch angles $\lesssim 16.5°$ at the first crossing of the centre plane. Now from the previous discussion the initial equatorial pitch angle is given by $\alpha_0 = \sin^{-1}(B_z/B_c)^{3/2}$ where B_c is the field strength at the point of creation, so that $\alpha_0 \lesssim 16.5°$ translates to $B_c/B_z \lesssim 2.31$ or to $|z^*| \lesssim 2.0$ using our simple model of the tail field. Thus, this approximation should be valid for particles created over more than two-thirds of the total thickness of the plasma sheet in a more realistic three-dimensional field model.

It has therefore been established that approximate conservation of $v_{\|_0} L$, along with conservation of μ, may be used to specify completely the motion of the majority of the lithium ions, to an accuracy of $\sim 20\%$, from the point where the trajectory first crosses the centre plane to some Earthward equatorial position where the ions are to be detected.

Having discussed the behaviour of J for ions with small equatorial pitch angle, for which $v_{\|}$ dominates the motion, we now turn to consider those ions created close to the centre plane with large μ, and hence for which $v_\perp$ dominates.

These ions are confined to the weak field region close to the centre plane throughout their motion, where the field strength runs approximately as the distance squared away from the equator, and hence will execute

simple harmonic motion along the field lines, as in Fig. 2, in an effective parabolic potential well (the approximation taken above for the small equatorial pitch angle ions corresponds to motion in a square potential well). We would therefore expect that ions which are created sufficiently close to the centre plane that their motion is simple harmonic along the field would conserve J, at least in the de Hoffman–Teller frame where U_E is zero. The effect of the presence of drifts comparable to the particle speed can be seen in Fig. 10, where $J^*(\frac{1}{2})$ is plotted, in the same equatorial pitch angles that have been created successively closer to the centre plane. We can see that for all the examples shown, $J^*(\frac{1}{2})$ is largest when calculated over the first half bounce period where U_E is largest, and decreases as the ion moves in towards the Earth where U_E is smaller. If J is conserved in the de Hoffman–Teller frame, then the amount by which it decreases over the trajectory must then be given approximately by the last term in equation (31). The final steady values for $J^*(\frac{1}{2})$ which correspond to motion in the dipole dominated region where U_E is small (e.g. Fig. 2) should then be just given by $J(\frac{1}{2})$ calculated in the de Hoffman–Teller frame.

Since for ion motion that is confined to a region sufficiently close to the centre plane, the field may be taken to be one-dimensional and the ion motion as sinusoidal, we may obtain approximate analytical values for J calculated in both the de Hoffman–Teller ($U_E = 0$) and the Earth ($\mathbf{U}_E \simeq E_y/B_z\hat{\mathbf{x}}$) frames.

We will first calculate $J(\frac{1}{2})$ for the first half bounce period, in the de Hoffman–Teller frame. Ions are created at height z_c in a field taken approximately to be $\mathbf{B} = (B'_x z, 0, B_z)$ where B'_x is the constant field x component gradient in the z direction, and B_z is constant. In the de Hoffman–Teller frame, the parallel velocity on creation is not zero (see Fig. 6), and maximizes at the centre plane, and hence is given by

$$v_{\parallel H}(t) = v_{\parallel 0} \sin \omega_{\parallel} t \tag{34}$$

where $\omega_{\parallel}$ is the bounce frequency and $t = 0$ at the

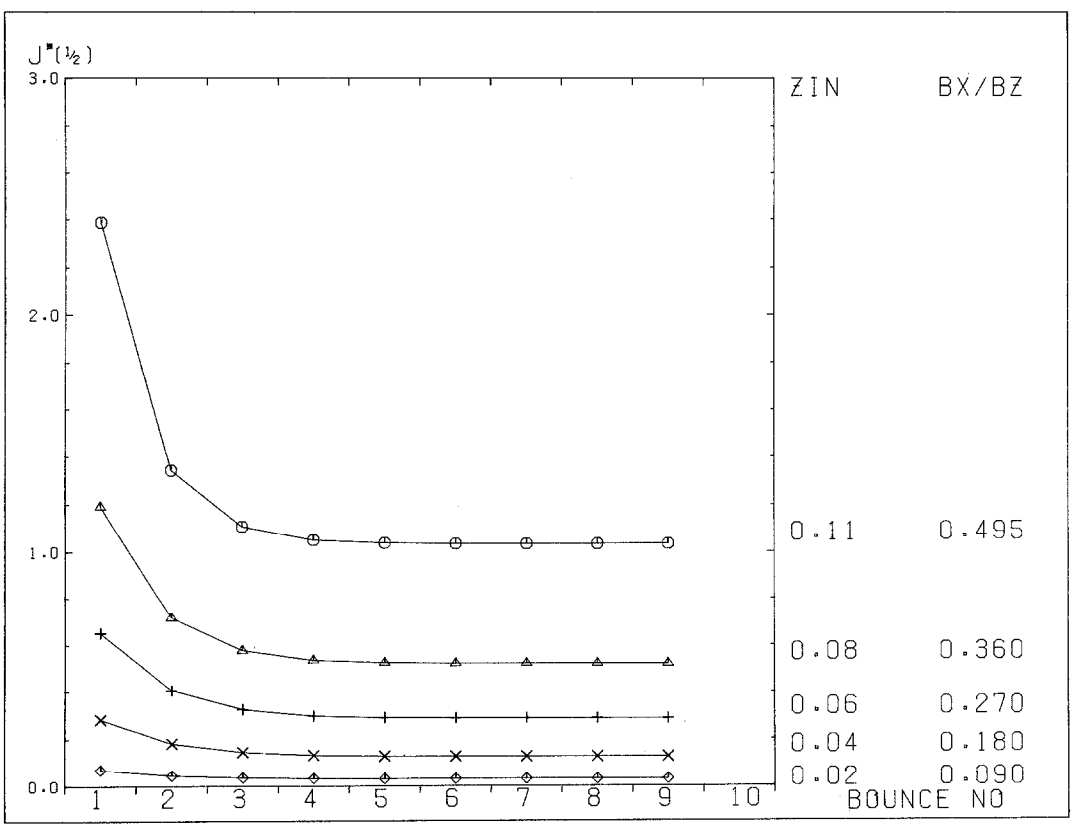

FIG. 10. THE NORMALIZED SECOND ADIABATIC INVARIANT CALCULATED OVER SUCCESSIVE HALF-BOUNCE PERIODS $J^*(\frac{1}{2})$ IS SHOWN PLOTTED IN THE SAME FORMAT AS THE PREVIOUS FIGURES FOR THE TRAJECTORIES OF LARGE PITCH ANGLE IONS THAT ARE CREATED CLOSE TO THE CENTRE PLANE.

mirror point $z_m \geqslant z_c$. Note that this just corresponds to sinusoidal motion in the moving frame, where $v_\parallel$ is zero at the creation point, and maximizes just after the ion crosses the centre plane (as in Fig. 2). $J(\frac{1}{2})$ is then easily obtained in this frame, as

$$J_H(\tfrac{1}{2}) = \int_0^{\pi/\omega_\parallel} v_{\parallel H}^2(t)\, dt = \frac{v_{\parallel 0}^2}{\omega_\parallel}\frac{\pi}{2}. \tag{35}$$

Then since

$$B \simeq B_z + \frac{B_x'^2 z^2}{2B_z} + \ldots. \tag{36}$$

in the limit $z < \dfrac{B_z}{B_x'}$

the restoring force on the ions as they execute S.H.M.

$$F = -\mu \nabla B = -\mu \frac{\partial B}{\partial z}$$

gives the bounce frequency

$$\omega_\parallel^2 = \frac{B_x'^2}{B_z}\frac{\mu}{m} \tag{37}$$

then since $\mu/m = v_{\perp_c}^2/B_c$ and $v_{\perp_c} = E/B_c$, expanding binomially for B_c gives

$$\omega_\parallel = \frac{B_x' v_T}{\sqrt{2B_z}}\left(1+\tfrac{3}{4}\left(\frac{B_{x_0}' z_c}{B_z}\right)^2\right)^{-1} \tag{38}$$

where v_T is the transformation speed E/B_z, and the ion speed v during the first half bounce period (see Fig. 6). Also from conservation of μ

$$\frac{v^2}{B(z_m)} = \frac{v_{\perp_c}^2}{B_c}$$

so that expanding binomially yields $z_m = \sqrt{3}\, z_c$. Then since

$$v_{\parallel 0}^2 = v^2\left(1-\frac{B_z}{B(z_m)}\right) \simeq v^2 \frac{3}{2}\frac{B_x'^2 z_c^2}{B_z^2} \tag{39}$$

by conservation of μ and expanding for z_c we can obtain $J_H(\frac{1}{2})$ in terms of known quantities. Substitution of equations (38) and (39) into (35) gives

$$J_H(\tfrac{1}{2}) = \frac{\pi}{2}\cdot\frac{3}{\sqrt{2}}\frac{vB_x' z_c^2}{B_z}\left(1+\frac{3}{4}\left(\frac{B_x' z_c}{B_z}\right)^2\right). \tag{40}$$

On normalizing $J_H(\frac{1}{2})$ to the typical units discussed in Section 2, we can estimate the final steady values of the curves shown in Fig. 10, corresponding to ion motion in regions where U_E is small, from the initial values of the creation height z_c^* and the values of $B_x^{*\prime}$ and B_z^* at the centre plane at $x = -20\ R_E$ in our two-dimensional model. Note that since $B_z/B_x' \simeq 0.22$ at this point, and $z_m \simeq \sqrt{z_c}$ we are limited, for instance, by equation (36) to applying this analytical estimate to ions created at $|z_c^*| < 0.13$. Within this range our analytical estimate of $J_H(\frac{1}{2})$ is in good agreement with the numerical values, differing by $\sim 6\%$ for $|z_c^*| = 0.11$, decreasing to $\sim 1.5\%$ for ions created closer to the centre plane, where $|z_c^*| < 0.06$. This result then implies that J is indeed preserved for these ions when calculated in the de Hoffman–Teller frame, and hence any approximate invariant obtained from J should also be calculated in this frame.

Before discussing such an invariant, however, it still remains to be shown that the shape of the curves in Fig. 10 is due to $J^*(\frac{1}{2})$ being obtained in a moving frame. To do this we once again consider an ion moving in the de Hoffman–Teller frame with parallel speed $v_{\parallel H}(t)$ given by equation (34), but now calculate $J(\frac{1}{2})$ in a frame moving with speed $v_T = E_y/B_z$ so that it will be just given by the terms in equation (31). Since we have already obtained $J_H(\frac{1}{2})$, and assuming that the middle term will approximately integrate to zero over a half bounce period, we need only express the last term as a function of known parameters. Using the expansion for the field (equation (36)) this term when taken over a half bounce period becomes

$$J_c(\tfrac{1}{2}) = v_T^2 \int_0^{\pi/\omega_\parallel} \frac{B_x'^2}{B_z^2} z^2\, dt. \tag{41}$$

Then, since the motion is simple harmonic in the z direction

$$z(t) = z_m \cos \omega_\parallel t \tag{42}$$

with $t = 0$ at the mirror points in the de Hoffman–Teller frame z_m. The convective contribution to $J(\frac{1}{2})$ becomes

$$J_c(\tfrac{1}{2}) = \frac{\pi v_T^2}{2\omega_\parallel}\frac{B_x'^2}{B_z^2} z_m^2. \tag{43}$$

We wish to compare the magnitude of $J_c(\frac{1}{2})$ obtained for any half bounce period with the magnitude of $J_H(\frac{1}{2})$ which is obtained for the first half bounce period and is constant throughout the trajectory.

From equations (35) and (43) we have

$$\frac{J_c(\frac{1}{2})}{J_H(\frac{1}{2})} = \frac{v_{Te}^2}{v_{\parallel 0}^2}\frac{\omega_\parallel}{\omega_{\parallel e}}\frac{B_{xe}'^2}{B_{ze}^2} z_{me}^2 = \frac{v_{Te}^2}{v_{\parallel 0e}^2}\frac{B_{xe}'^2}{B_{ze}^2} z_{me}^2 \tag{44}$$

where subscript e denotes quantities evaluated for half bounce periods earthward of the creation distance, and hence $v_{\parallel 0}^2/\omega_\parallel = v_{\parallel 0e}^2/\omega_{\parallel e}$ by conservation of J_H.

Now since close to the centre plane $v_H(t) \simeq \mathrm{d}z/\mathrm{d}t$,

equations (34) and (42) give $z_m \simeq v_{\|o}/\omega_{\|}$, so that

$$\frac{J_c(\frac{1}{2})}{J_H(\frac{1}{2})} = \frac{2v_{Te}^2}{v_{\perp 0e}^2} = \frac{2v_{Te}^2}{v_{\perp_0}^2}\frac{B_z}{B_{ze}} \tag{45}$$

using equation (37) and conservation of μ. Then since $v_{Te} \simeq E/B_{ze}$ and $v_{\perp_0} \simeq E/B_z$

$$\frac{J_c(\frac{1}{2})}{J_H(\frac{1}{2})} = 2\left(\frac{B_z}{B_{ze}}\right)^3. \tag{46}$$

Having already obtained values for $J_H(\frac{1}{2})$ corresponding to the ions created at the various z_c^*, we can now estimate the curves shown in Fig. 10 analytically. The various values of B_{ze}, taken at the point where the ion crosses the centre plane during each half bounce period, represent intermediate values of the range of B_{ze} encountered by the ion between mirror points, and as such are approximations to the required average B_{ze}.

A further source of error in this procedure is the assumption that the middle term in equation (31) integrates to zero over each half bounce period. This is only approximately valid since v_T, that is, U_E, is not constant along the ion trajectories. Nevertheless it is found that equation (46) provides a reasonably accurate estimate of $J(\frac{1}{2})$, differing from the numerical values by less than $\sim 20\%$ for ions created with $|z_c^*| \leqslant 0.11$.

It has thus been shown that, for ions created sufficiently close to the centre plane, $J(\frac{1}{2})$ and hence J are well preserved if calculated in the de Hoffman–Teller frame. The approximate longitudinal invariant of the motion for these ions has therefore been derived using conservation of J in the de Hoffman–Teller frame, and conservation of μ. This derivation may be found in the Appendix, where it is shown that

$$M = v_{\|o}\left(\frac{B_z}{\left(\frac{\partial B_x}{\partial z}\right)^2}\right)^{1/4} \tag{47}$$

is conserved, where all the parameters refer to values at centre plane crossings.

In Fig. 11 M^* is plotted for the various trajectories with the same format as the previous figures. Since from the Appendix we see that J is not simply proportional to M, no attempt has been made here to compare the absolute magnitudes of the two quantities. It is clear from the figure that M^* is well preserved for ions created within the limit $|z_c^*| < 0.13$ that is required for the motion to be simple harmonic along the field. Ions created at larger z^* do not conserve M^* until the velocity along the field becomes more sinusoidal (see Fig. 5 of Paper 1) in the dipolar region of the field. It is found that M^* is conserved to better than 20% over the trajectories of ions created with $|z_c^*| < 0.17$, where $|B_x|/B_z < 0.77$.

The equatorial values for the velocity components, obtained from equations (27) and (28), can now be transformed to appropriate values earthwards of the creation region by means of the approximate invariants for $v_{\|_0}$ given by equations (33) and (47), and by conservation of μ. Small pitch angle ions, created where $|B_x|/B_z > 1.0$ in the two-dimensional field, will lie on the line in velocity space given by

$$\left(\frac{v_{\|_e}L_e}{L}\right)^2 + \left(v_{\perp_e}\left(\frac{B_z}{B_{ze}}\right)^{1/2}\right)^2 = \left(\frac{E_y}{B_z}\right)^2 \tag{48}$$

and large pitch angle ions, created where $|B_x|/B_z \leqslant 0.77$ on the line given by

$$v_{\|e}^2 \frac{\left(\frac{\partial B_x}{\partial z}\right)}{\left(\frac{\partial B_x}{\partial z}\right)_e}\left(\frac{B_{ze}}{B_z}\right)^{1/2} + \left(v_{\perp_e}\left(\frac{B_z}{B_{ze}}\right)^{1/2}\right)^2 = \left(\frac{E_y}{B_z}\right)^2 \tag{49}$$

where subscript e denotes quantities obtained at some equatorial position earthwards of the release, and all other quantities refer to the first crossing of the centre plane. We see then that the circle given by equation (28) on which the ions appear in velocity space as they first cross the centre plane transforms to the above ellipses during the subsequent earthward motion.

The above limits on $|B_x|/B_z$ at the creation point can, using equation (27), be translated to limits on the equatorial pitch angles of ions as they first cross the centre plane. Hence we require that at the first crossing of the centre plane, $\alpha_0 < 36.5°$ for the small pitch angle approximation to apply (in the two-dimensional field), and $\alpha_0 > 45°$ for the large pitch angle approximation. These limits on α_0 at the first crossing can then be approximately transformed to values appropriate to the ring current region, using equations (48) and (49). For our two-dimensional field, if we take the point where the ions first cross the centre plane to be located at $x \simeq -20\ R_E$, and then map the above equatorial values to $x \simeq -8\ R_E$, the two limits become $\alpha_{0e} < 38.5°$ and $\alpha_{0e} > 67.1°$ respectively.

Finally, we can use equations (48) and (49) to determine the equivalent limits on α_{0_e} in the ring current region appropriate for the Earth's three-dimensional field, remembering that the small pitch angle limit at the first crossing of the centre plane $\alpha_0 < 16.5°$ in this case. Taking the field line length L to have changed by approximately the same amount as in our two-dimensional model, but the centre plane field in the ring current region ($x = -8\ R_E$) to have increased by a factor ~ 2.5, gives the small pitch angle limit of $\alpha_{0e} < 26.7°$.

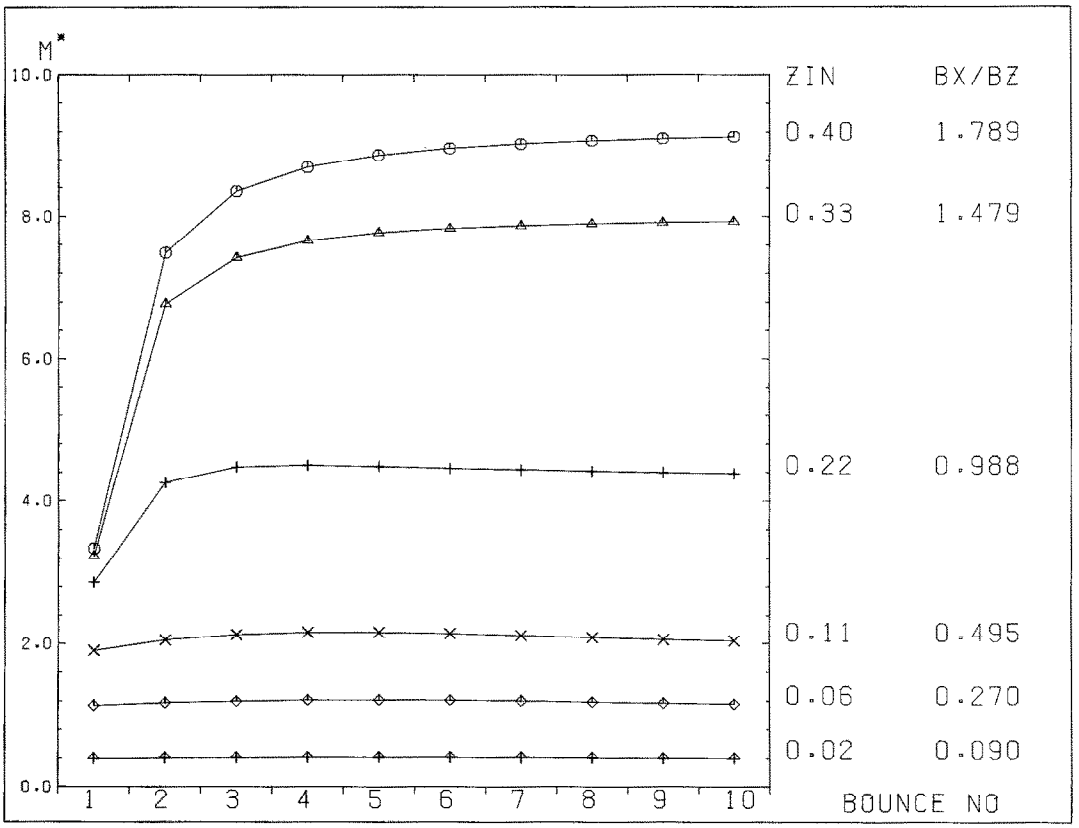

FIG. 11. THE APPROXIMATE LONGITUDINAL INVARIANT, M^*, HAS BEEN CALCULATED FOR THE TRAJECTORIES OF IONS CREATED CLOSE TO THE CENTRE PLANE, INCLUDING THOSE REFERRED TO IN THE PREVIOUS FIGURE, AND IS SHOWN IN THE SAME NORMALIZED UNITS AND FORMAT.

Now, in the large pitch angle limit, the equatorial pitch angle α_{0_e} earthwards of the release distance is given in terms of the pitch angle α_0 at the first crossing by

$$\tan \alpha_{0e} = \tan \alpha_0 \left(\frac{B_{ze}}{B_z}\right)^{3/4} \left(\frac{\dfrac{\partial B_x}{\partial z}}{\left(\dfrac{\partial B_x}{\partial z}\right)_e} \right)^{1/2} \tag{50}$$

from equation (47) and conservation of μ. We now wish to compare the equatorial pitch angles found in the dipolar region resulting from ion motion in a two-dimensional and a three-dimensional field. The field parameters near $x = -20\,R_E$ are taken to be the same in both fields, so that the initial equatorial ion pitch angle α_0 is also unchanged, then

$$\frac{\tan \alpha_{0e_2}}{\tan \alpha_{0e_3}} = \left(\frac{B_{ze_2}}{B_{ze_3}}\right)^{3/4} \left[\frac{\left(\dfrac{\partial B_x}{\partial z}\right)_{e_3}}{\left(\dfrac{\partial B_x}{\partial z}\right)_{e_2}} \right]^{1/2} \tag{51}$$

where the subscripts 2 and 3 denote the parameters appropriate for the two- and three-dimensional fields. The two- and three-dimensional fields at the centre plane in the dipolar region are given by $B_z = B_{z_2} \simeq k_2/x^2$, and $B_z = B_{z_3} \simeq k_3/x^3$ respectively, where k_2 and k_3 are the field dipole strengths. Substituting into equation (51) gives

$$\frac{\tan \alpha_{0e_2}}{\tan \alpha_{0e_3}} = \left(\frac{k_2 x_e}{k_3}\right)^{3/4} \left(\frac{3k_3}{2k_2 x_e}\right)^{1/2} = \left(\frac{3}{2}\right)^{1/2} \left(\frac{B_{ze_2}}{B_{ze_3}}\right)^{1/4} \tag{52}$$

and since $B_{ze_3}/B_{ze_2} \simeq 2.5$ at $x = -8\,R_E$, the above just yields $\tan \alpha_{0e_2} \simeq \tan \alpha_{0e_3}$. In general then, the pitch angles with which ions created close to the centre plane arrive in the ring current region in the Earth's field will not differ from those calculated here for the two-dimensional model. On the other hand, we have seen that results calculated in the two-dimensional model underestimate the pitch angles of ions created in the

strong field region further from the centre plane, such that $\tan \alpha_{0e_3} = \sqrt{2.5} \tan \alpha_{0e_2}$ in the ring current region. Also, since $v_{\perp 0e}$ is $\sim\sqrt{2.5}$ larger in the three-dimensional field, the above argument suggests that the speeds of large pitch angle particles will be $\sim\sqrt{2.5}$ larger also, whereas the speeds of small pitch angle particles will not be significantly different as the field line lengths in the two- and three-dimensional fields are similar.

To summarize these results we shall compare the velocities and pitch angles of ions arriving in the ring current region calculated first by numerical integration of their guiding centre trajectories in the two-dimensional model and second, using the approximate invariants described in this section. Equatorial values appropriate to a chosen reference field line in the ring current region are obtained from the local values of $v_\perp$ and $v_\parallel$ as each trajectory intersects the reference field line by conservation of μ and approximate conservation of energy (valid since $v \gg U_E$ in this region). The asterisks on Fig. 12 show the result of applying such a procedure to the trajectories of ions that were created

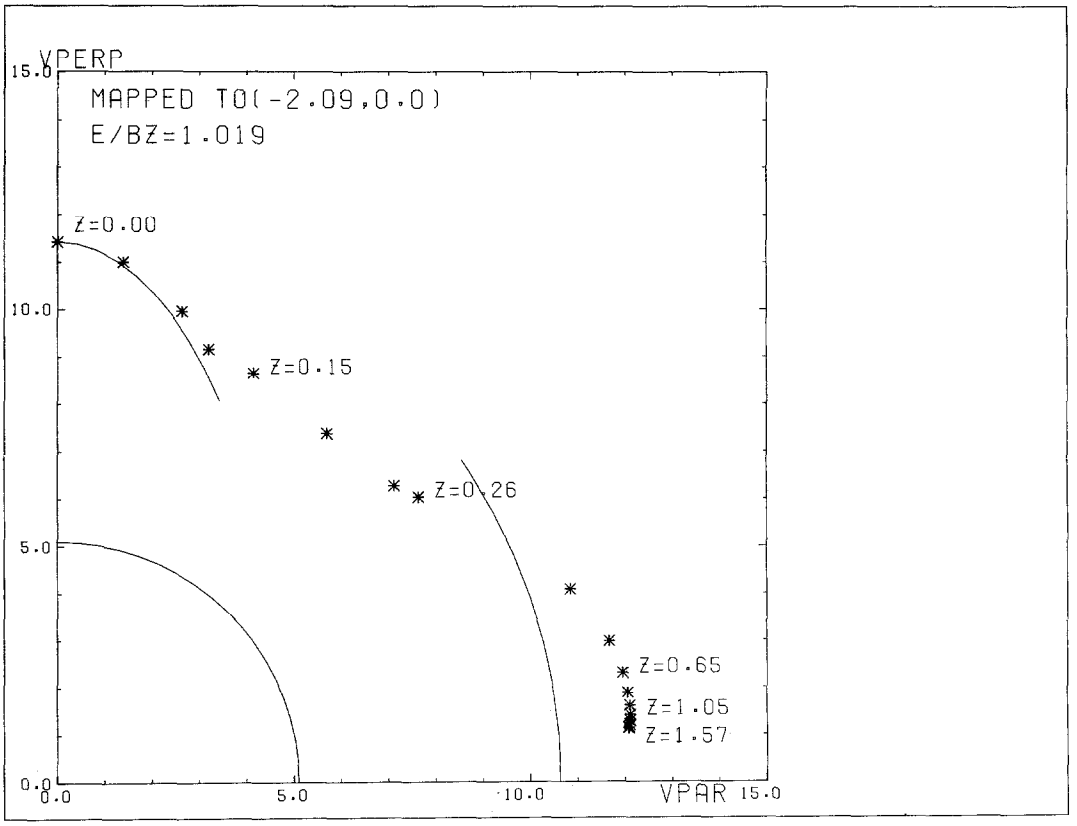

FIG. 12. THE NORMALIZED SPEEDS AND EQUATORIAL PITCH ANGLES OF IONS CROSSING A SPECIFIED RING CURRENT FIELD LINE (WHICH INTERSECTS THE CENTRE PLANE AT $x \simeq -8\,R_E$, OR $x^* = -2.09$) ARE PLOTTED AS ASTERISKS IN VELOCITY SPACE.

The equatorial pitch angle was calculated from local velocity values on crossing this field line by transforming at constant energy and μ. The ion trajectories referred to here are just those used in Fig. 6, and once again since the ions were created non-uniformly in z^* the normalized creation height of various ions is also given. A quadrant of a circle which has a radius given by the normalized field-line speed at the centre plane at $x = -20\,R_E$ (also shown in Fig. 6) is plotted in order to represent the properties of the ions as they first cross the centre plane. The result of mapping this circle to $x = -8\,R_E$, $z = 0$, by means of the approximate longitudinal invariants and conservation of μ is shown for both the small and large pitch angle approximations described in the text, within the limits for which these approximate invariants are conserved, to better than $\sim 20\%$. Velocities are again normalized to the characteristic units discussed in Section 2, so that one unit is typically ~ 10 km s^{-1}.

non-uniformly over the plasma sheet height (the trajectories used here are just those used to produce Fig. 6). Here the normalized equatorial velocity components were obtained for a reference field line which passes through the equator at $x \simeq -8\ R_E$ ($x^* = -2.09$). The quadrant of the circle in Fig. 6, given by equation (28), is also plotted here for comparison, showing the degree of acceleration which has taken place, and the normalized height above the centre plane at which various ions were created is also given. It is immediately clear that, as we would expect from the results in Section 3 and those given in Paper 1 (e.g. Fig. 6), the speeds of ions arriving in the ring current region are not strongly dependent on the initial creation height. The typical values here of $v^* \simeq 12$ translates to $v = 120$ km s^{-1} using our typical units from Section 2 and $E_y = 0.2$ mV m^{-1}, corresponding to an energy of ~ 525 eV for lithium ions. The pitch angle, however, does depend sensitively on the initial creation height, and we can see that ions created over the majority of the centre plane appear at small pitch angles, which, from Fig. 6 of Paper 1 can be seen to lie in the range 5–15°.

We can now compare these numerical results with predictions made by means of the approximate invariants and conservation of μ. First, the ions are assumed to lie on the sphere in velocity space given by equation (28) and the circle plotted here as they first cross the centre plane. This sphere is then transformed according to equations (48) and (49) using the field values at $x = -8\ R_E$, and the resulting ellipses are plotted on Fig. 12 as solid lines, within the limits of validity of the approximate invariants given above. It is then clear from Fig. 12 that the analytical estimates described in this section provide a reasonable approximation to the numerical results.

We have therefore shown in this section that, given the special conditions of the lithium releases whereby test ions are created at rest, during quiet times such that the ion motion is adiabatic, then the subsequent equatorial ion properties earthwards of the release may be obtained analytically for any given quiet time model of the field.

Finally, we shall briefly discuss the implications of the above results for the motion of lithium test ions during disturbed times. Just preceding a substorm, the plasma sheet thickness at the release distance is observed to decrease, from the quiet time value of $\sim 6\ R_E$ to $\sim$ 1–2 R_E or less (e.g. Hones *et al.*, 1971). A new neutral line is believed to form in the vicinity of the release, resulting in fast plasma flows in the centre plane with speeds $\sim$ 100–800 km s^{-1}, which are far in excess of those observed during quiet times (Cattell and Mozer, 1984). Clearly ions created tailwards of this neutral line $\mathbf{E} \wedge \mathbf{B}$ drift onto field lines which no longer originate on the Earth, and hence move tailwards and are lost. We will therefore only discuss the properties of ions created Earthwards of this neutral line.

Since within the thinned plasma sheet, the weak field region, where $|B_x| \lesssim B_z$, will be much narrower than at quiet times, almost all of the lithium test ions will be created in strong field regions with small magnetic moment. These ions then $\mathbf{E} \wedge \mathbf{B}$ drift to the centre plane as before, but the first interaction with the centre plane will not conserve μ, since we have seen from equation (10) that ion behaviour becomes less adiabatic as the field radius of curvature is reduced. Instead, the motion described by Speiser (1965) is more appropriate, where it is shown that, on entering the weak field region, the ions execute a half turn about a small but finite B_z and then emerge at various pitch angles which are closely aligned to the field. The energy gained in this interaction may, however, still be inferred by the de Hoffman–Teller frame transformation (e.g. Cowley, 1980) and is just such that the field-aligned speed of the ions is increased by approximately twice the field line speed at the centre plane.

After the first interaction with the plasma sheet, the ions therefore still form a closely field-aligned beam, as at quiet times, but now with much higher speeds, typically from ~ 200 km s^{-1} to over 1000 km s^{-1}. The earthward moving ions now fill the loss-cone, but since in our case this is only $\sim \frac{1}{2}°$ it is expected that nearly all these ions mirror close to the Earth and return to the centre plane. Their subsequent behaviour will then depend effectively on the field line radius of curvature at the region where the ions again cross the centre plane. If the field at this distance is approximately dipolar, then ion motion will be adiabatic on this and subsequent current sheet interactions. Hence the ion behaviour in the x–z plane after the first current sheet interaction will be qualitatively similar to that shown in Fig. 1, and the properties of ions arriving in the ring current region are gven by the above analysis. However, it is possible that, under more disturbed conditions, the plasma sheet will thin over considerable distances earthwards of the release. Significant pitch angle scattering will then occur for several of the ion interactions with the current sheet. In this case, only a rough estimate may be made of the energy with which the ions arrive in the ring current region, since most energy is still likely to be gained on the first interaction with the current sheet.

We may now use these estimates of the energy gained by the ions to calculate their cross-tail displacement during Earthward convection, since any net energy gain must be associated with a displacement in the direction of the ambient electric field (e.g. equation (6)). During quiet times, we have seen that the energy gained

by the ions is ~ 1 keV, which corresponds to acceleration along a small fraction of the typical cross-tail potential of ~ 50 kV, and hence to a cross-tail displacement of $\lesssim 1\ R_E$. However, since this energy gain is much larger during disturbed times, it is possible that the cross-tail displacement may also increase significantly. For instance, given flow speeds at the centre plane at the release distance of $\sim 500\ \mathrm{km\ s^{-1}}$, the energy gained after the first interaction with the current sheet alone is $\simeq 37$ keV. This must be compared with cross-tail potentials of typically 100–200 kV during disturbed times, giving cross-tail drifts which may be a substantial fraction of the tail width.

6. CONCLUSIONS

In this paper we have used the guiding centre approximation to integrate the trajectories of lithium test ions as they convect earthwards from the release point at $\sim 20\ R_E$ to the ring current region, using a simple two-dimensional model of the quiet-time nightside magnetosphere. It is found that the ion energies in the ring current region depend principally on the field line speed where their trajectories first cross the centre plane, but is not sensitive to the distance from the centre plane at which the ions are created. The expected energies in the ring current region are ~ 500 eV–1 keV. The ion pitch angles, however, depend strongly on the creation height, and specifically on the field ratio $|B_x|/B_z$ at the point of creation.

Ions that are created close to the centre plane, where $B_z \gtrsim |B_x|$ are created at large μ and appear at correspondingly large pitch angles. The majority of ions created over the rest of the plasma sheet thickness, where $|B_x| > B_z$, are accelerated in $v_{\|}$ as they cross the centre plane and hence arrive at the ring current region with small pitch angles, typically in the range ~ 5–$15°$.

In Section 4 we have conducted an investigation into the conditions required for the breakdown of guiding centre theory. Parameters which quantify the extent to which the guiding centre approximation is valid along the ion trajectories were derived, and it was shown that this approximation is least satisfied as small pitch angle ions first cross the centre plane. Numerical results were then presented which could be conveniently used to translate the magnitudes of these parameters into an estimate of the amount of pitch angle scattering expected to occur in the region where behaviour is least adiabatic. Then, since the parameters were shown to scale with the cross-tail electric field, it was deduced that, for lithium ions, pitch angle scattering due to non-adiabatic behaviour would be small over the typical range of quiet time values for the electric field.

Finally, in Section 5 the behaviour of the second adiabatic invariant J was investigated numerically, in order to determine approximate invariants of the motion. These invariants could then be used with conservation of μ to predict the equatorial speeds and pitch angle of ions at any point earthwards of the release, given the equatorial values at the release distance itself. These values were estimated analytically, for the special case of ions created at rest, by using a simple one-dimensional approximation for the field which allowed transformation to an $E_y = 0$ frame (the de Hoffman–Teller frame). It was then shown that using this procedure, the speeds and pitch angles of the ions at the ring current region could be predicted, to a reasonable accuracy, without recourse to numerical integration, and hence for any given model field.

Acknowledgement–This work was performed while one of the authors (S.C.C.) was supported by a U.K. Science and Engineering Research Council Studentship.

REFERENCES

Behannon, K. W. (1968) Mapping of Earth's bow shock and magnetic tail by *Explorer* 33. *J. geophys. Res.* **73**, 907.

Behannon, K. W. (1970) Geometry of the geomagnetic tail. *J. geophys. Res.* **75**, 743.

Cattell, C. A. and Mozer, F. S. (1984) Substorm electric fields in the Earth's magnetotail, in *Magnetic Reconnection in Space and Laboratory Plasmas* (Edited by Hones, E. W. Jr.), p. 208. AGU, Washington, D.C.

Chapman, S. C. and Cowley, S. W. H. (1984) Acceleration of lithium test ions in the quiet time geomagnetic tail. *J. geophys. Res.* **89**, 7357.

Cowley, S. W. H. (1980) Plasma populations in a simple open model magnetosphere. *Space Sci. Rev.* **26**, 217.

de Hoffman, F., and Teller E. (1950) Magneto-hydrodynamic shocks. *Phys. Rev.* **80**, 692.

Fairfield, D. H. (1979) On the average configuration of the geomagnetic tail. *J. geophys. Res.* **84**, 1950.

Gray, P. C. and Lee, L. C. (1982) Particle pitch angle diffusion due to nonadiabatic effects in the plasma sheet. *J. geophys. Res.* **87**, 7445.

Hones, E. W., Jr., Asteridge, J. R. and Bame, S. J. (1971) Time variations of the magnetotail plasma sheet at 18 R_E determined from concurred observations by a pair of Vela satellites. *J. geophys. Res.* **76**, 4402.

Krimigis, S. M., Haerendel, G., McEntire, R. W., Paschmann, G. and Bryant, D. A. (1982) The Active Magnetospheric Particle Tracer Explorers (AMPTE) program, EOS. *Trans. Am. geophys. Union* **63**, 843.

Mihalov, J. D., Colburn, D. S., Currie, R. G. and Sonnett, C. P. (1968) Configuration and reconnection of the geomagnetic tail. *J. geophys. Res.* **73**, 943.

Northrop, T. G. (1963) The adiabatic motion of charged particles. *Interscience.*

Northrop, T. G. and Teller, E. (1960) Stability of the adiabatic motion of charged particles in the Earth's field. *Phys. Rev.* **117**, 215.

Reiff, P. H., Spiro, R. W. and Hill, T. W. (1981) Dependence of polar cap potential drop on interplanetary parameters. *J. geophys. Res.* **86**, 7639.

Speiser, T. W. (1965) Particle trajectories in model current sheets, *J. geophys. Res.* **70**, 4219.

APPENDIX

Here we shall derive an approximate longitudinal invariant of the motion of large pitch angle ions that remain close to the centre plane throughout their trajectories.

The field at a distance s along a field line close to the centre plane may be taken as

$$\mathbf{B}(s) = (B_x' s, 0, B_z) \tag{A1}$$

for reasons given in the text, where B_z is constant and B_x' is the constant gradient of the x component of the field. An approximation for the second adiabatic invariant J will first be obtained for particle motion in this field, in the de Hoffman–Teller ($E = 0$) frame, since it has been shown that in general J will only be conserved in this frame. The ion motion will then be symmetric in $v_\parallel$ about the centre plane, so that

$$J = \oint v_\parallel \, ds = 4 \int_0^{s_m} v_\parallel \, ds \tag{A2}$$

where s is the distance along the field from the centre plane and s_m denotes the mirror point in the de Hoffman–Teller frame.

Then conserving energy and μ gives

$$v_\parallel^2(s) = v^2\left(1 - \sin^2 \alpha_0 \frac{B(s)}{B_z}\right). \tag{A3}$$

An expression for s may be obtained from the approximate field (1) as

$$\frac{B^2(s)}{B_z^2} = 1 + \frac{B_x'^2 s^2}{B_z^2} = 1 + \left(\frac{s}{L}\right)^2 \tag{A4}$$

where $L = \dfrac{B_z}{B_x'}$.

Then since the mirror points are such that $v_\parallel = 0$

$$\frac{B(s_m)}{B_z} = \frac{1}{\sin^2 \alpha_0} \tag{A5}$$

so that from equation (4)

$$\left(\frac{s_m}{L}\right)^2 = \left(\frac{1}{\sin^4 \alpha_0} - 1\right). \tag{A6}$$

Using

$$y = \frac{s}{s_m} = \frac{s}{L\left(\dfrac{1}{\sin^4 \alpha_0} - 1\right)^{1/2}} \tag{A7}$$

the integral (2) becomes

$$J = 4 v s_m \int_0^1 dy \left\{1 + \sin^2 \alpha_0 \left[1 - y^2 \left(\frac{1}{\sin^4 \alpha_0} - 1\right)\right]^{1/2}\right\}^{1/2}. \tag{A8}$$

Then confining the discussion to large equatorial pitch angles, such that $s_m/L \lesssim 1$ which implies $\alpha_0 \gtrsim 60°$, then since $0 \leqslant y \leqslant 1$ over the integral (8) expanding binomially gives

$$\begin{aligned} J &\simeq 4 v s_m \int_0^1 dy \left\{1 - \sin^2 \alpha_0 \left[1 + \frac{y^2}{2}\left(\frac{1}{\sin^4 \alpha_0} - 1\right)\right]\right\}^{1/2} \\ &= 4 v_{\parallel_0} s_m \int_0^1 dy \left(1 - \frac{(1 + \sin^2 \alpha_0)}{\sin^2 \alpha_0} \frac{y^2}{2}\right)^{1/2} \\ &\simeq 4 v_{\parallel_0} s_m \int_0^1 dy (1 - y^2)^{1/2} \quad \text{since } \sin \alpha_0 \simeq 1 \\ &\simeq \pi v_{\parallel_0} s_m. \end{aligned} \tag{A9}$$

To replace s_m in equation (9) use equation (6)

$$\begin{aligned} J &\simeq \pi v_{\parallel_0} L \frac{(1 - \sin^4 \alpha_0)^{1/2}}{\sin^2 \alpha_0} \\ &\simeq \sqrt{2} \pi v_{\parallel_0} L \cos \alpha_0 \quad \text{since } \sin \alpha_0 \simeq 1 \\ &= J_A \end{aligned} \tag{A10}$$

conservation of μ gives

$$\frac{v \sin \alpha_0}{\sqrt{B_z}} \simeq \frac{v}{\sqrt{B_z}} = \mu_A \tag{A11}$$

so

$$\frac{J_A}{\mu_A} = \sqrt{2\pi} \sqrt{B_z} L \cos^2 \alpha_0 \tag{A12}$$

must also be conserved.

Eliminating $\cos \alpha_0$ between equations (10) and (12) gives

$$\frac{J_A}{(J_A/\mu_A)^{1/2}} = 2^{1/4} \sqrt{\pi} v_{\parallel_0} \frac{L^{1/2}}{B_z^{1/4}}. \tag{A13}$$

Then, since $L = B_z/B_x'$, and at the centre plane $B_x' = \partial B_x/\partial z$, the approximate invariant becomes

$$\begin{aligned} M &= v_{\parallel_0} \left(\frac{B_z}{\left(\dfrac{\partial B_x}{\partial z}\right)^2}\right)_0^{1/4} \\ &= \frac{1}{2^{1/4}\sqrt{\pi}} \frac{J_A}{(J_A/\mu_A)^{1/2}}. \end{aligned} \tag{A14}$$